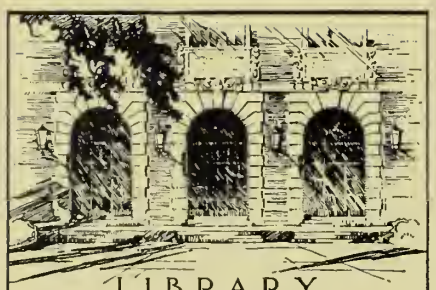

Antenna Laboratory

Technical Report No. 9

EFFECTIVE PERMEABILITY OF SPHEROIDAL SHELLS

by

E. J. Scott
and
R. H. DuHamel

15 April 1956

Contract AF33(616)-3220
Project No. 6(7-4600)Task 40572
WRIGHT AIR DEVELOPMENT CENTER

Electrical Engineering Research Laboratory
Engineering Experiment Station
University of Illinois
Urbana, Illinois

ABSTRACT

The static field solutions for a spheroidal shell placed in a uniform magnetic field are derived. The solutions are then used to calculate the effective permeability of prolate and oblate spheroidal shells. The results, in the form of sets of curves showing the variation of the effective permeability with the shell thickness and the ratio of major to minor axis, are applied in the comparison of various types of cores for ferrite loop antenna applications.

CONTENTS

	Page
Abstract	ii
1. Introduction	1
2. The Prolate Spheroidal Shell	3
3. The Oblate Spheroidal Shell	17
4. Application to Loop Antenna Design	32
5. Conclusions	39
6. Acknowledgment	40

ILLUSTRATIONS

Figure Number		*Page*
1.	Uniform Magnetic Field Applied on a Prolate Spheroidal Shell	4
2.	Prolate Spheroidal Coordinates	4
3a.	μ_e versus μ for a Solid Prolate Spheroid ($b'/b = 0$) for Various Length-to-Diameter Ratios	10
3b.	μ_e versus μ for a Prolate Spheroidal Shell ($b'/b = .5$) for Various Length-to-Diameter Ratios	11
3c.	μ_e versus μ for a Prolate Spheroidal Shell ($b'/b = .8$) for Various Length-to-Diameter Ratios	12
3d.	μ_e versus μ for a Prolate Spheroidal Shell ($b'/b = .9$) for Various Length-to-Diameter Ratios	13
4a.	μ_e versus b'/b for a Prolate Spheroidal Shell ($c/b = 1.25$) for Various μ	14
4b.	μ_e versus b'/b for a Prolate Spheroidal Shell ($c/b = 2$) for Various μ	14
4c.	μ_e versus b'/b for a Prolate Spheroidal Shell ($c/b = 5$) for Various μ	15
4d.	μ_e versus b'/b for a Prolate Spheroidal Shell ($c/b = 10$) for Various μ	16
5.	Uniform Magnetic Field Applied to an Oblate Spheroidal Shell with an Elliptical Loop Placed in the xz Plane	18
6.	Oblate Spheroidal Coordinates	18
7a.	μ_e versus μ for a Solid Oblate Spheroid ($a'/a = 0$) for Various Diameter-to-Thickness Ratios	22
7b.	μ_e versus μ for an Oblate Spheroidal Shell ($a'/a = .5$) for Various Diameter-to-Thickness Ratios	23
7c.	μ_e versus μ for an Oblate Spheroidal Shell ($a'/a = .8$) for Various Diameter-to-Thickness Ratios	24
7d.	μ_e versus μ for an Oblate Spheroidal Shell ($a'/a = .9$) for Various Diameter-to-Thickness Ratios	25
8a.	μ_e versus a'/a for an Oblate Spheroidal Shell ($c/a = 1.25$) for Various μ	26
8b.	μ_e versus a'/a for an Oblate Spheroidal Shell ($c/a = 2$) for Various μ	26
8c.	μ_e versus a'/a for an Oblate Spheroidal Shell ($c/a = 5$) for Various μ	27

ILLUSTRATIONS (Cont.)

Figure Number		*Page*
8d.	μ_e versus a'/a for an Oblate Spheroidal Shell ($c/a = 10$) for Various μ	28
9.	Uniform Magnetic Field Applied to an Oblate Spheroidal Shell with a Circular Loop Placed in the yz Plane	29
10.	μ_e versus μ for a Solid Oblate Spheroid for Various Diameter-to-Thickness Ratios (c/a)	31
11.	μ_e versus a'/a for an Oblate Spheroidal Shell ($c/a = 2$) for Various μ	31
12.	Curves Showing the Length-to-Diameter Ratio, c/b, of a Solid Prolate Spheroid Required to Produce the Same Effective Permeability as a Solid Cylindrical Rod with a Length-to-Diameter Ratio of L/D	32
13.	Plot of $(A\mu_e)^2$ versus c/b for the Prolate Spheroid and c/a for the Oblate Spheroid	35
14.	Plot of $(A\mu_e)^2$ versus c/b and c/a for the Solid Prolate and Oblate Spheroidal Cores with c Held Constant	36
15.	Plot of $(A\mu_e)^2$ versus c/b for a Prolate Spheroidal Core with c and the Core Volume Held Constant	38

1. INTRODUCTION

For flush- or nearly flush-mounted loop antennas a ferromagnetic core is commonly used to increase the efficiency of the antenna. The recent development of low loss, high permeability ferrite materials has made possible the design of ferrite loops with efficiencies equal to those of much larger air core loops. In the design of a ferrite core, the engineer must decide on the shape, size, and weight, as well as the type of material for the core. This work was undertaken to provide a basis for the comparison of cores of various shapes, sizes and weights. Since the radiation resistance of a ferrite loop is proportional to the square of the effective permeability of the core and the loop area, the efficiency of the loop is strongly dependent on these two quantities.

In the following, the results of the derivation and evaluation of exact expressions for the effective permeability of prolate and oblate spheroidal shells are given and are used to compare various types of spheroidal shells. Now, admittedly, the spheroid is not a practical shape for a ferrite core. However, two practical shapes, the cylindrical rod and the circular disk may be approximated by the prolate and oblate spheroids, respectively. The determination of the effective permeability of a body involves the solution of a magnetostatic boundary value problem. (The static solution is accurate for bodies with dimensions which are small compared to the wavelength.) Exact solutions for the rod, tube or disk would be prohibitively difficult to obtain since the surfaces of these bodies do not coincide with a coordinate surface for any of the coordinate systems for which Laplace's equation is separable. On the other hand, spheroidal harmonics may be used to obtain exact solutions for the spheroid or spheroidal shell. Thus, instead of obtaining approximate answers for the desired practical shapes, we have obtained exact answers for approximate shapes.

With regard to previous work, an exact solution for the general solid ellipsoid, of which the spheroid is a special case, was obtained many years ago. Extensive numerical results for the ellipsoid and approximate results for the cylindrical rod have been given in recent years.[1,2] In these references, the results are given in the form of a demagnetization factor, D, from which the effective permeability, μ_e,

1. Bozorth, R. M. and Chapin, D. M. "Demagnetizing Factors of Rods," *J. App. Phys.*, *13*, (1942) p. 320.
2. Osborn, J. A. "Demagnetizing Factors of the General Ellipsoid," *Phys. Rev.*, *67* (1945) p. 351.

may be determined by

$$\mu_e = \frac{\mu}{1 + D(\mu-1)}$$

where μ is the relative permeability of the core material. For the ellipsoid, D is independent of μ since a uniform field exists in an ellipsoid when it is inserted into a uniform field. However, since D is a function of μ for an ellipsoidal or spheroidal shell, the advantage of using D is lost. Thus we will be concerned only with μ_e.

2. THE PROLATE SPHEROIDAL SHELL

The problem to be solved is defined as follows. With reference to Fig. 1a, consider an applied uniform static magnetic field of intensity H_0 in the negative z direction which produces a total magnetic flux, Φ_0, through the circular wire loop of radius b.

Next, consider the total flux, Φ_s, passing through the loop when a prolate spheroidal shell of permeability μ and dimensions shown in Fig. 1b is placed inside the loop. The objective is to calculate the ratio Φ_s/Φ_0 which is defined here as the effective permeability, μ_e, of the shell.

According to magnetostatic theory

$$\overline{H} = -\nabla\varphi \tag{1}$$

and

$$\nabla^2\varphi = 0 \tag{2}$$

where H is the total magnetic field and φ is a scalar function of position. Thus the solution may be obtained by solving Laplace's equation, subject to the appropriate boundary conditions.

It is convenient to use prolate spheroidal coordinates[3] $(\xi,\eta,\overline{\varphi})$ in the solution (see Fig. 2). The outside surface of the shell is defined by the prolate spheroid with semi axes b and c. The family of spheroids which includes this surface is given by

$$\frac{\rho^2}{c_2^2(\eta^2-1)} + \frac{z^2}{c_2^2\eta^2} = 1 \tag{3}$$

where

$$x = \rho \sin\overline{\varphi},\quad y = \rho\cos\overline{\varphi}$$

$$c_2^2 = c^2 - b^2$$

$$1 \le \eta < \infty\ .$$

---

3. Refer to W. R. Smythe, "Static and Dynamic Electricity," McGraw Hill, 1939; pp. 165-167.

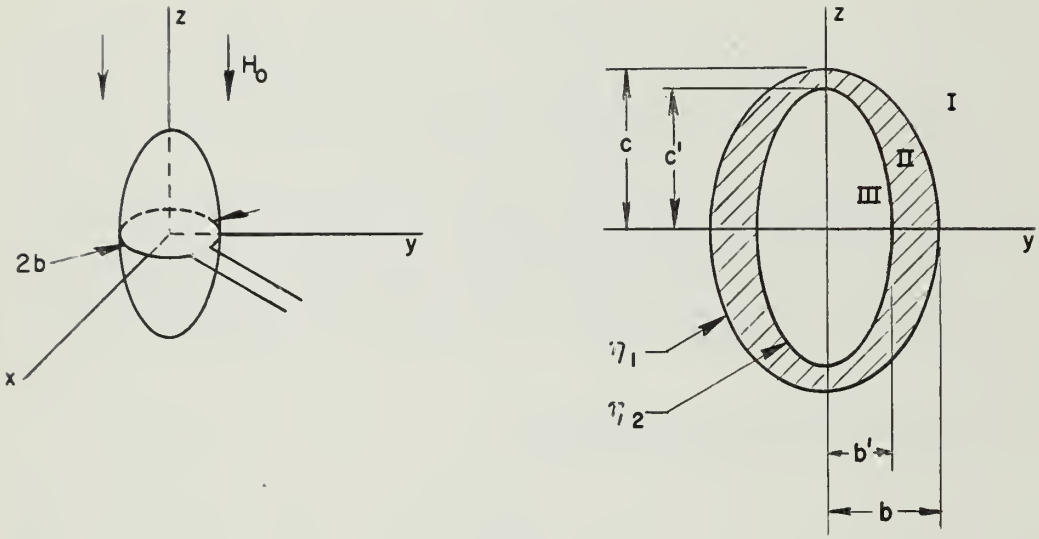

Figure 1. Uniform Magnetic Field Applied on a Prolate Spheroidal Shell

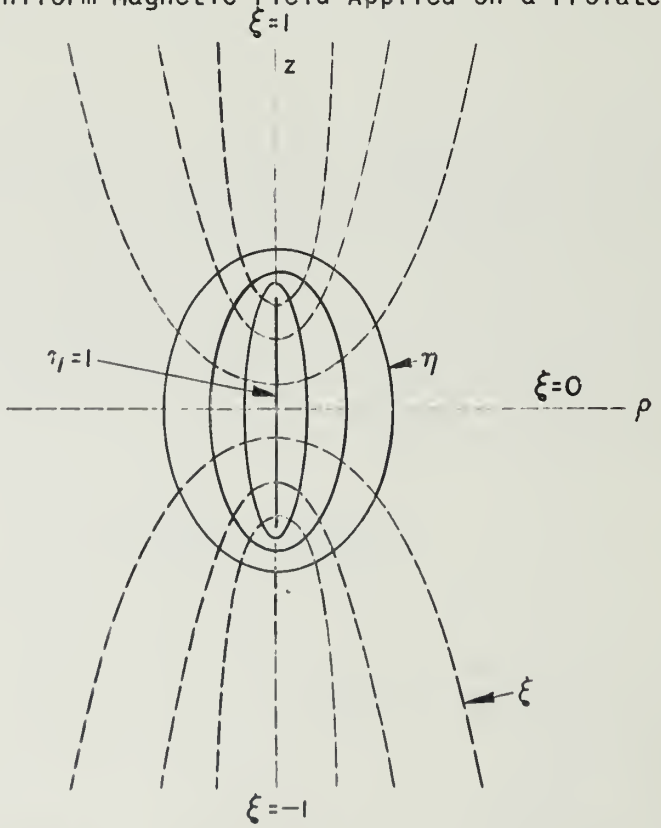

Figure 2. Prolate Spheroidal Coordinates

The outside surface, η_1, is defined by

$$\eta_1 = \frac{c}{c_2} = \frac{1}{\sqrt{1-(b/c)^2}} \quad . \tag{4}$$

Let the inside surface, η_2, of the shell be defined by

$$\eta_2 = \frac{\sqrt{c^2-Kb^2}}{c_2} = \eta_1 \sqrt{1-K(b/c)^2}, \quad 0 \leq K \leq 1 \quad . \tag{5}$$

It is then found that

$$\frac{b'}{b} = \sqrt{1-K} \quad . \tag{6}$$

and

$$\frac{b'}{c'} = \frac{b}{c}\sqrt{\frac{1-K}{1-K(b/c)^2}} \quad . \tag{7}$$

The orthogonal family of coordinate surfaces are the hyperboloids defined by

$$\frac{\rho^2}{c_2^2(1-\xi^2)} + \frac{z^2}{c_2^2\xi^2} = 1 \tag{8}$$

where

$$-1 \leq \xi \leq 1 \quad .$$

The cylindrical coordinates ρ and z are related to the prolate spheroidal coordinates ξ and η by

$$\begin{aligned} z &= c_2\eta\xi \\ \rho &= c_2[(1-\xi^2)(\eta^2-1)]^{1/2} \quad . \end{aligned} \tag{9}$$

The prolate spheroidal harmonics which are solutions of Laplace's equation are of the form

$$\varphi = [A'P_n^m(\xi) + B'Q_n^m(\xi)]\,[AP_n^m(\eta) + BQ_n^m(\eta)] \times [C\cos m\overline{\varphi} + D\sin m\overline{\varphi}] \tag{10}$$

where P_n^m and Q_n^m are the associated Legendre functions of the first and second kind, respectively. Since there is no $\overline{\varphi}$ variation for this problem, m must equal zero. Also, since $Q_n(1) = \infty$, the $Q_n(\xi)$ functions cannot be used.

The potential corresponding to the applied uniform field is

$$\varphi_o = H_o z = H_o\, r \cos\theta \tag{11}$$

where r and θ are the spherical coordinates. Now as $\eta \to \infty$

$$r^2 = \rho^2 + z^2 \to c_2^2\, \eta^2$$

so that $\eta \to r/c_2$ and $\xi = z/c_2\eta \to z/r = \cos\theta$. Thus ξ can enter only as $P_1(\xi) = \xi$ and the potential of the total field in Region I must be of the form

$$\begin{aligned} \varphi_S^I &= P_1(\xi)\,[AP_1(\eta) + BQ_1(\eta)] \\ &= \xi[A\eta + B(\eta \coth^{-1}\eta - 1)] \\ &= \frac{z}{c_2}\left[A + B(\coth^{-1}\eta - \frac{1}{\eta})\right] . \end{aligned} \tag{12}$$

Now, as $z \to \infty$, $\eta \to \infty$, then $\eta^{-1} \to 0$ and $\coth^{-1}\eta \to 0$ so that A may be evaluated by equating Eqs. 11 and 12

$$A = c_2 H_o . \tag{13}$$

Therefore, for Region I, the potential is

$$\varphi_S^I = \xi[c_2 H_o \eta + B(\eta \coth^{-1}\eta - 1)]. \tag{14}$$

In Region II between the prolate spheroids corresponding to $\eta = \eta_1$ and $\eta = \eta_2$ the potential is of the form

$$\varphi_S^{II} = \xi[C\eta + D(\eta \coth^{-1}\eta - 1)] \tag{15}$$

and in Region III, since the potential must be finite, the potential is

$$\varphi_S^{III} = E\xi\eta . \tag{16}$$

The four unknown constants, B, C, D, and E, may be evaluated by using the following boundary conditions

$$\varphi^{I} = \varphi^{II}, \quad \frac{\partial \varphi^{I}}{\partial \eta} = \mu \frac{\partial \varphi^{II}}{\partial \eta} \text{ at } \eta = \eta_1$$

$$\varphi^{II} = \varphi^{III}, \quad \mu \frac{\partial \varphi^{II}}{\partial \eta} = \frac{\partial \varphi^{III}}{\partial \eta} \text{ at } \eta = \eta_2 , \tag{17}$$

where μ is the relative permeability of the shell material. These conditions yield four equations from which the four unknown constants may be determined. The solution yields the following expressions for the potentials:

$$\varphi_s^{I} = \xi\eta\left[c_2 H_0 + \eta_1(\eta_1^2-1)\left\{(\mu-1)(\coth^{-1}\eta_2 - \coth^{-1}\eta_1) + \frac{(\mu-1)\eta_1^2+1}{\eta_1(\eta_1^2-1)} - \frac{(\mu-1)\eta_2^2+1}{\eta_2(\eta_2^2-1)}\right\}\right.$$
$$\left. \times \left(\coth^{-1}\eta - \frac{1}{\eta}\right)D\right]$$

$$\varphi_s^{II} = \xi\eta\left[\coth^{-1}\eta - \frac{1}{\eta} + \frac{(\mu-1)\eta_2^2+1}{(\mu-1)\eta_2(\eta_2^2-1)} - \coth^{-1}\eta_2\right]D \tag{18}$$

$$\varphi_s^{III} = \frac{\mu\xi\eta}{(\mu-1)\eta_2(\eta_2^2-1)} D$$

where

$$D = \frac{c_2 H_0}{\left[\left(\coth^{-1}\eta_1 - \frac{1}{\eta_1}\right) - \coth^{-1}\eta_2 + \frac{(\mu-1)\eta_2^2+1}{(\mu-1)\eta_2(\eta_2^2-1)}\right.}$$
$$\left. - \left(\coth^{-1}\eta_1 - \frac{1}{\eta_1}\right)\eta_1(\eta_1^2-1)\left\{(\mu-1)(\coth^{-1}\eta_2 - \coth^{-1}\eta_1) + \frac{\eta_1^2(\mu-1)+1}{\eta_1(\eta_1^2-1)} - \frac{\eta_2^2(\mu-1)+1}{\eta_2(\eta_2^2-1)}\right\}\right]$$

Now the flux passing through the loop may be obtained by integrating the normal flux density over the circle enclosed by the loop. The normal flux density is

$$B_\xi = \mu H_\xi = -\mu[\nabla\varphi]_\xi = -\mu \frac{1}{c_2\eta} \left.\frac{\partial \varphi}{\partial \xi}\right|_{\xi = 0} .$$

The element of area on the equatorial plane is

$$da = c_2^2 \eta \, d\eta \, d\varphi \, .$$

Thus the total flux with the shell in position is

$$\Phi_s = \iint_{\text{loop area}} B_\xi \, da$$

$$\Phi_s = -\int_0^{2\pi} \int_1^{\eta_1} c_2 \mu \left. \frac{\partial \varphi_s}{\partial \xi} \right|_{\xi = 0} d\eta \, d\varphi$$

$$= -2\pi c_2 \left[\int_1^{\eta_2} \left. \frac{\partial \varphi_s^{III}}{\partial \xi} \right|_{\xi = 0} d\eta + \int_{\eta_2}^{\eta_1} \mu \left. \frac{\partial \varphi_s^{II}}{\partial \xi} \right|_{\xi = 0} d\eta \right] .$$

Substituting and integrating gives

$$\Phi_s = -\pi c_2 \mu D \left\{ (\eta_1^2 - 1)(\coth^{-1}\eta_1 - \coth^{-1}\eta_2) - (\eta_1 - \eta_2) + (\eta_1^2 - \eta_2^2) \left(\frac{(\mu-1)\eta_2^2 + 1}{(\mu-1)\eta_2(\eta_2^2 - 1)} \right) + \frac{1}{(\mu-1)\eta_2} \right\} .$$

For the shell removed, the total flux is

$$\Phi_0 = -\pi \, c_2^2 \, H_0 \, (\eta_1^2 - 1) \, .$$

Thus the effective permeability of the shell is

$$\mu_e \frac{\Phi_s}{\Phi_0} = \frac{\mu \left[\coth^{-1}\eta_1 - \coth^{-1}\eta_2 + \frac{(\eta_1 - \eta_2)(\eta_2\eta_1 + 1)}{(\eta_2^2 - 1)(\eta_1^2 - 1)} + \frac{1}{(\mu-1)\eta_2(\eta_2^2 - 1)} \right]}{\left[\left(\coth^{-1}\eta_1 - \frac{1}{\eta_1} \right) - \coth^{-1}\eta_2 + \frac{(\mu-1)\eta_2^2 + 1}{(\mu-1)\eta_2(\eta_2^2 - 1)} \right.}$$

$$\left. - \left(\coth^{-1}\eta_1 - \frac{1}{\eta_1} \right) \eta_1(\eta_1^2 - 1) \left\{ (\mu-1)(\coth^{-1}\eta_2 - \coth^{-1}\eta_1) + \frac{\eta_1^2(\mu-1)+1}{\eta_1(\eta_1^2 - 1)} - \frac{\eta_2^2(\mu-1)+1}{\eta_2(\eta_2^2 - 1)} \right\} \right] \qquad (19)$$

It is helpful to know several limiting values of μ_e. Consider first the case where $b'/b \to 0$, i.e., the effective permeability of a solid prolate spheroid. As $b'/b \to 0$, then $b'/c' \to 0$, $k \to 1$, and $\eta_2 \to 1$. By multiplying the numerator and denominator of Eq. 19 by (η_2^2-1) and dropping the terms that approach zero, it is found that for a solid core

$$\lim_{b'/b \to 0} \mu_e = \frac{\mu}{1+(\mu-1)(\eta_1^2-1)(\eta_1 \coth^{-1}\eta_1 - 1)}$$

$$= \frac{\mu}{1+(\mu-1)\frac{b^2}{c_2^2}\left(\frac{c}{c_2}\coth^{-1}\frac{c}{c_2} - 1\right)} \quad . \tag{20}$$

Next, consider the case where $\mu \to \infty$. It is easy to show that

$$\lim_{\mu \to \infty} \mu_e = \frac{c_2^2}{b^2\left(\frac{c}{c_2}\coth^{-1}\frac{c}{c_2} - 1\right)} \quad . \tag{21}$$

Notice that for $\mu = \infty$, μ_e is independent of η_2 and therefore independent of the shell thickness.

Finally, let the length-to-diameter ratio increase without limit (i.e., let $b/c \to 0$ or $\eta_1 \to 1$) and keep b'/b fixed. It is found that

$$\lim_{b/c \to 0} \mu_e = 1 + (\mu-1)\sqrt{1-\left(\frac{b'}{b}\right)^2} \quad . \tag{22}$$

The Illiac digital computer was used to calculate μ_e for various values of the parameters c/b, b'/b, and μ. Figures 3a to 3d illustrate the variation of μ_e with μ for various length-to-diameter ratios, c/b, for four different shell thicknesses. Figures 4a to 4d show the variation of μ_e with the shell thickness for various permeabilities and length-to-diameter ratios. It can readily be seen from these curves that solid cores are necessary only for low permeability materials. For example, notice that for a length-to-diameter ratio of five and a μ of 300 (which is not uncommon - Ferramic J has a μ of 500 for instance) that μ_e is reduced only from 17 to 14 when approximately 81 percent ($b'/b = .9$) of the core material is removed.

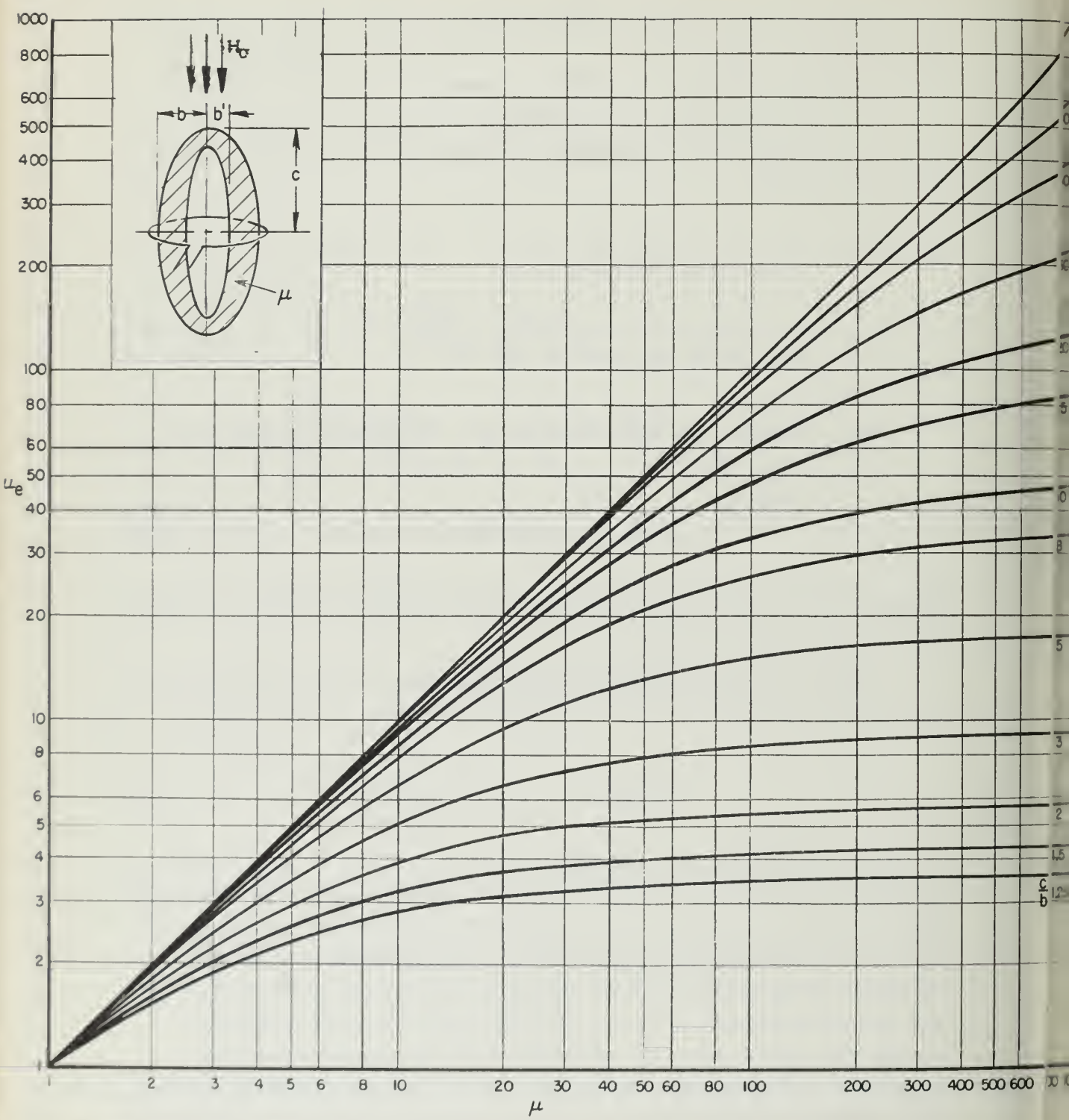

Figure 3a μ_e versus μ for a Solid Prolate Spheroid ($b'/b = 0$) for Various Length-to Diameter Ratios

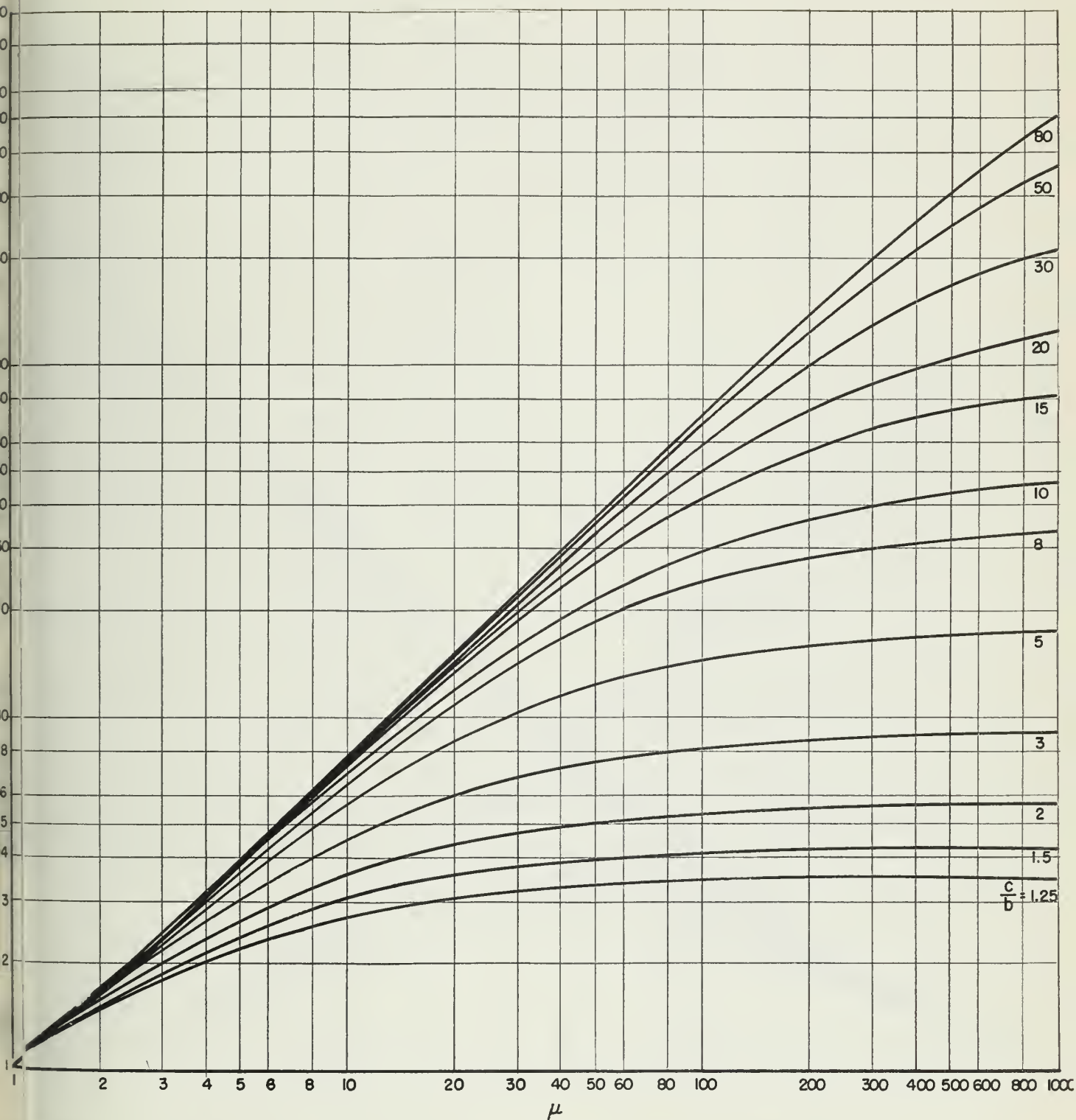

Figure 3b. μ_e versus μ for a Prolate Spheroidal Shell ($b'/b = .5$) for Various Length-to-Diameter Ratios

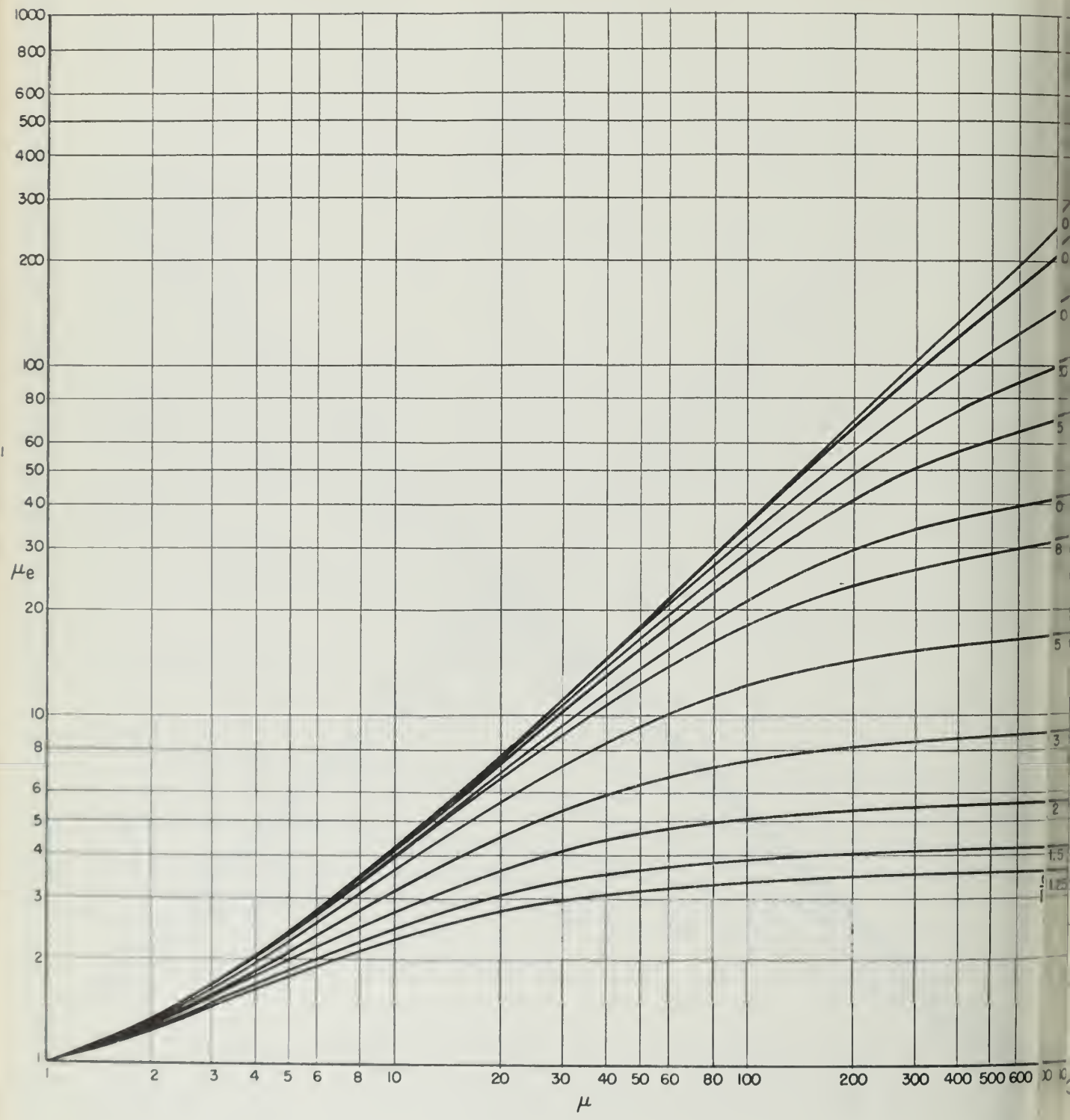

Figure 3c μ_e versus μ for a Prolate Spheroidal Shell ($b'/b = 8$) for Various Length-to-Diameter Ratios

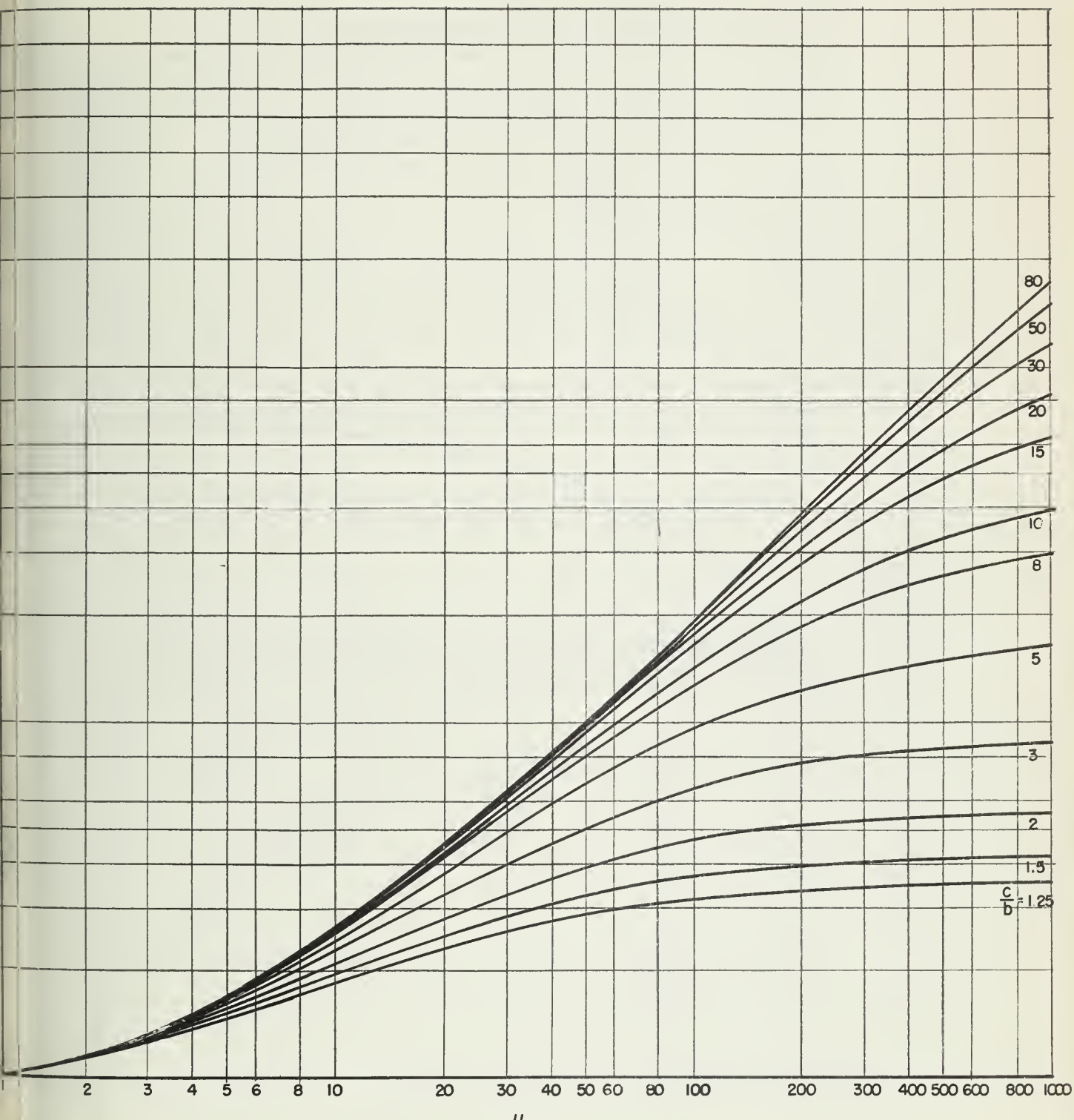

Figure 3d μ_e versus μ for a Prolate Spheroidal Shell ($b'/b = .9$) for Various Length-to-Diameter Ratios

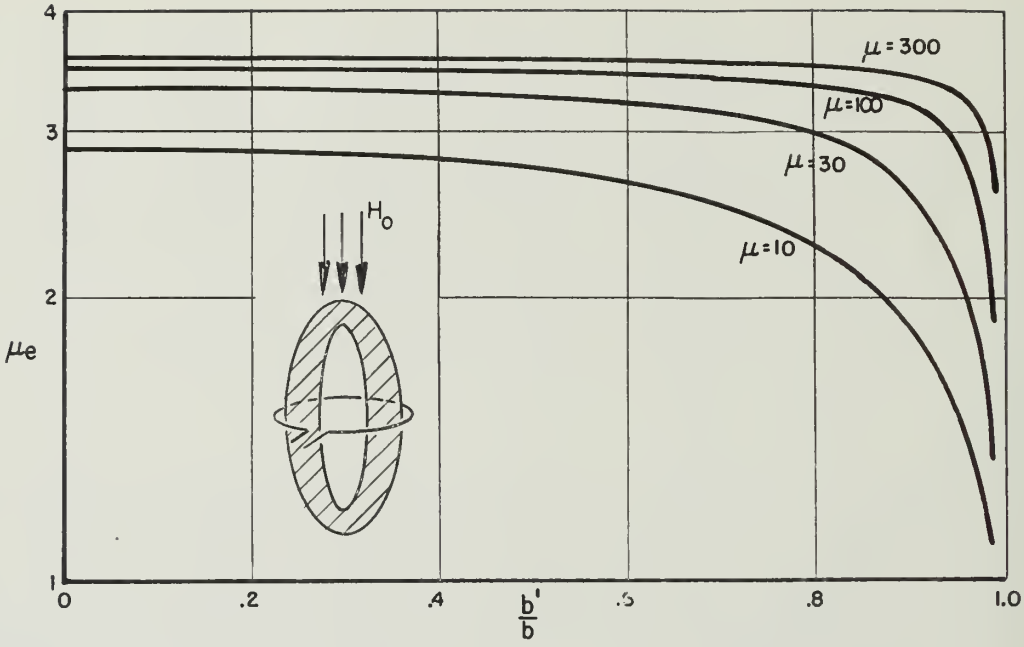

Figure 4a μ_e versus b'/b for a Prolate Spheroidal Shell ($c/b = 1.25$) for Various μ

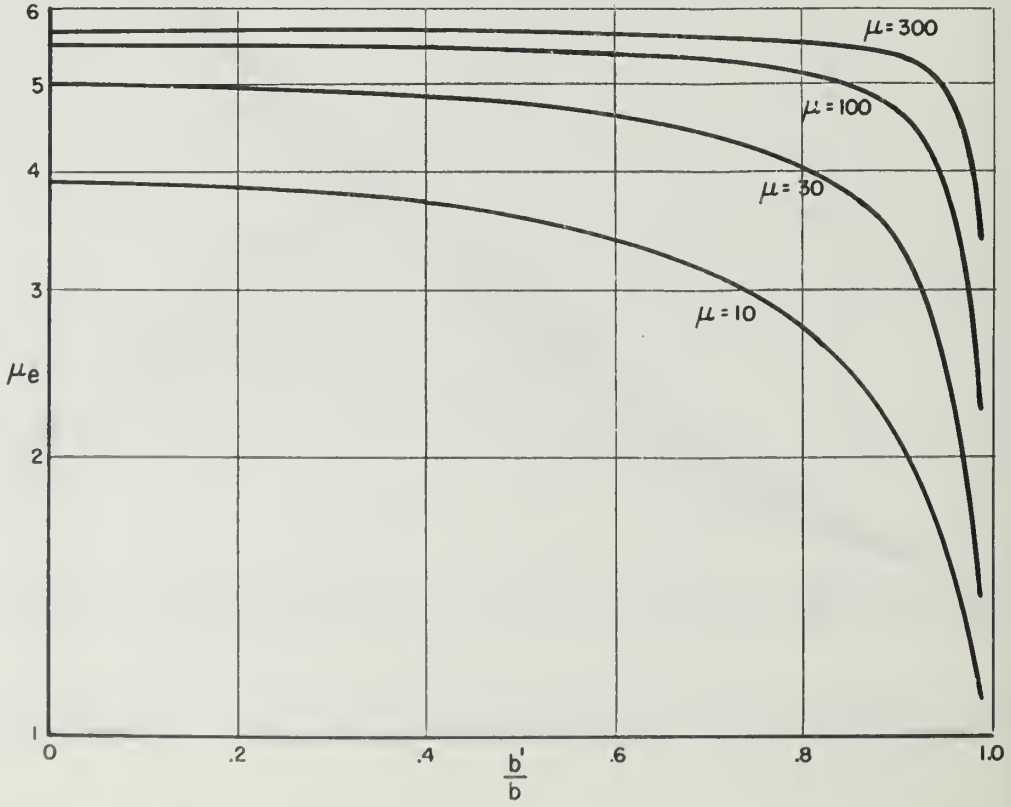

Figure 4b μ_e versus b'/b for a Prolate Spheroidal Shell ($c/b = 2$) for Various μ

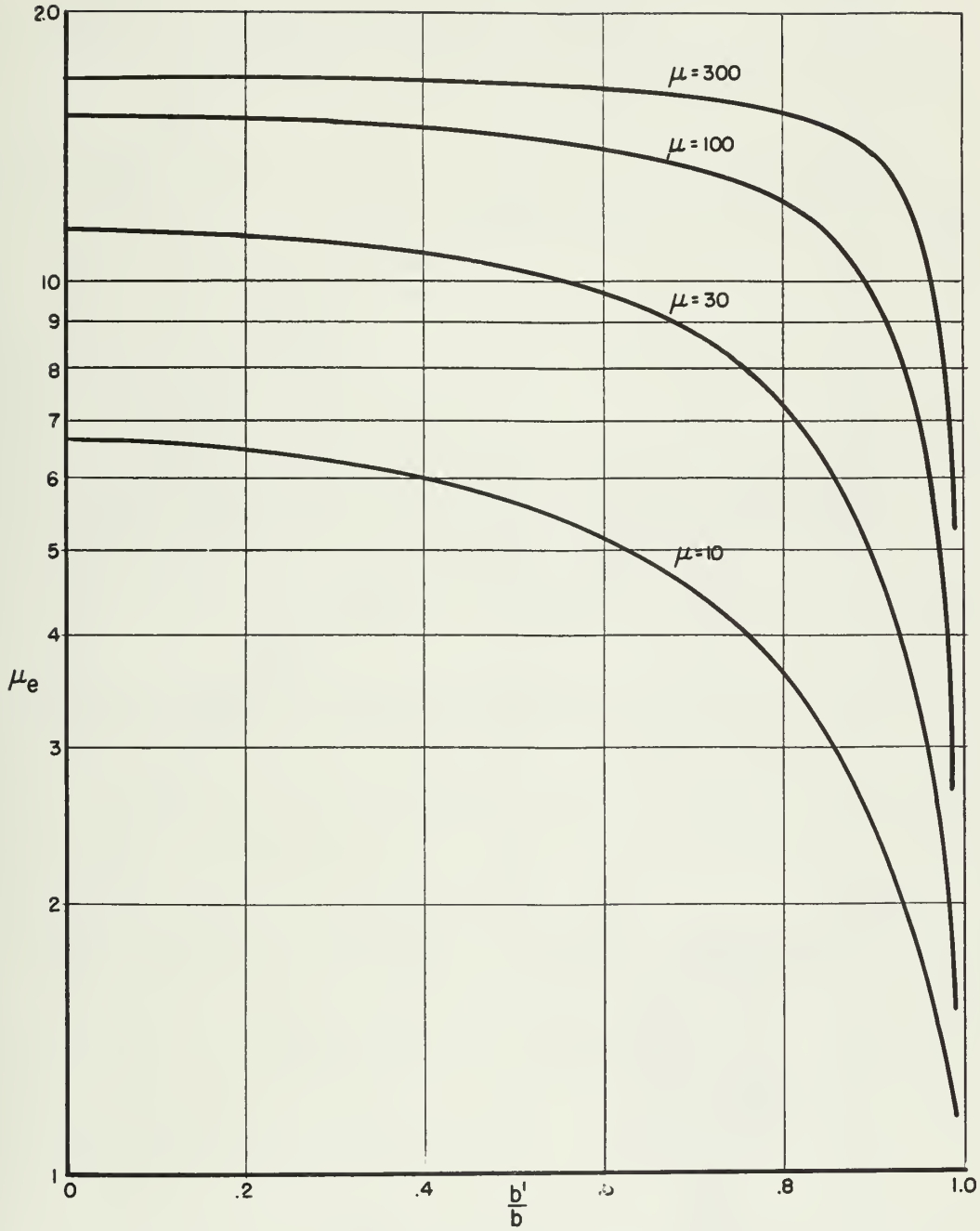

Figure 4c. μ_e versus b'/b for a Prolate Spheroidal Shell ($c/b = 5$) for Various μ

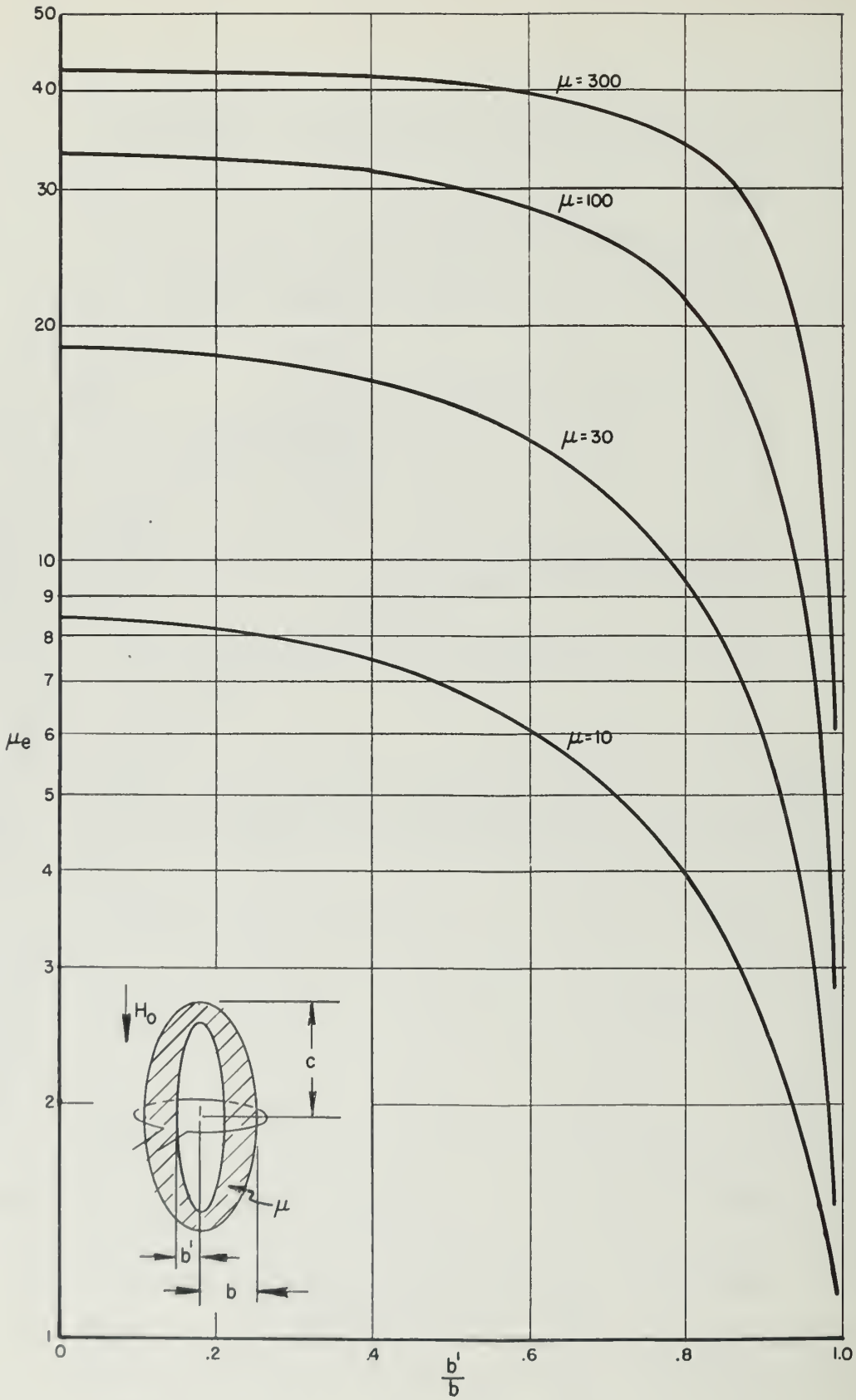

Figure 4d. μ_e versus b'/b for a Prolate Spheroidal Shell ($c/b = 10$) for Various μ

3. THE OBLATE SPHEROIDAL SHELL

In obtaining the solution for the oblate spheroidal shell (Fig. 5a) a procedure similar to that for the prolate case is followed. Referring to Fig. 5b, let the semi-axes a and c define the outer surfaces, and a′, c′, the inner surfaces of an oblate spheroidal shell. The family of oblate spheroids containing these surfaces is defined by the equation

$$\frac{x^2}{c_1^2\zeta^2} + \frac{\rho^2}{c_1^2(\zeta^2+1)} = 1, \tag{23}$$

where

$$y = \rho \cos \overline{\varphi}, \quad z = \rho \sin \overline{\varphi}$$

$$c_1^2 = c^2 - a^2, \quad 0 \leq \zeta \leq \infty.$$

From Eq. 23 and Fig. 5b it is seen that the value of ζ that defines the outer surface is

$$\zeta_1 = a/c_1 = 1/\sqrt{(c/a)^2 - 1}. \tag{24}$$

The inner surface can now be defined as

$$\zeta_2 = k(a/c_1) = k\zeta_1 \tag{25}$$

where $0 \leq k \leq 1$.

From the previous two definitions one obtains the relations

$$a'/a = k \text{ and } c'/c = \sqrt{1+(k^2-1)a^2/c^2}. \tag{26}$$

Corresponding to the spheroids are the family of orthogonal hyperboloids given by the equations

$$\frac{x^2}{c_1^2\xi^2} + \frac{\rho^2}{c_1^2(1-\xi^2)} = 1, \tag{27}$$

where $-1 \leq \xi \leq 1$.

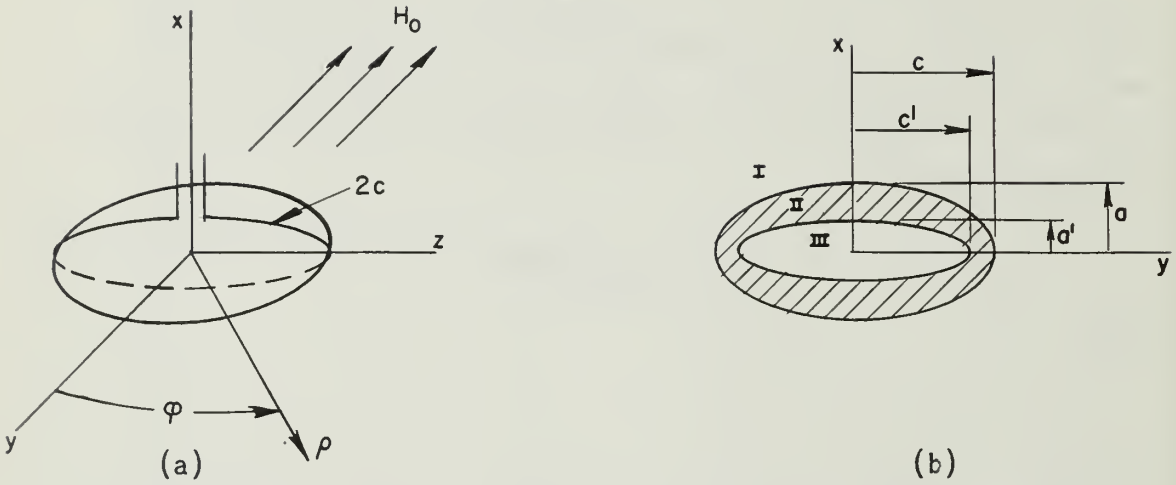

Figure 5. Uniform Magnetic Field Applied to an Oblate Spheroidal Shell with an Elliptical Loop Placed in the xz Plane

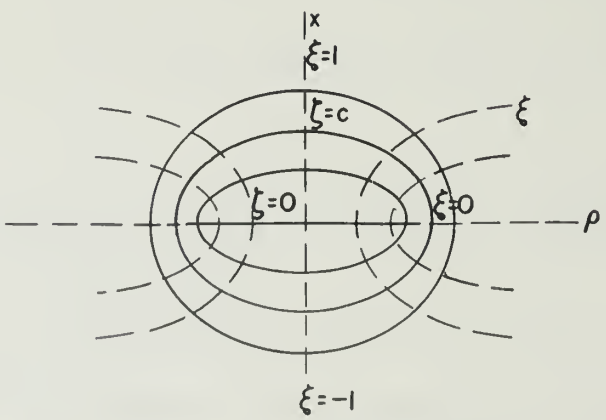

Figure 6 Oblate Spheroidal Coordinates

The oblate spheroidal coordinates of Fig. 6 are related to x and ρ by

$$\begin{aligned} x &= c_1 \zeta \xi, \\ \rho &= c_1 [(1+\zeta^2)(1-\xi^2)]^{1/2} . \end{aligned} \tag{28}$$

For the problem under consideration the oblate spheroidal harmonics are of the form

$$\varphi = [A' P_n^m(\xi) + B' Q_n^m(\xi)] [A P_n^m(j\zeta) + B Q_n^m(j\zeta)] \times [C \cos m\bar{\varphi} + D \sin m\bar{\varphi}] .$$

First, consider the case of Fig. 5a when the applied uniform magnetic field is in the negative y direction and an elliptical loop lying in the xz plane is placed around the spheroid. The potential of the applied field is then

$$\varphi_o = H_o y = H_o \rho \cos \bar{\varphi} .$$

As $\zeta \to \infty$ it may be shown that $\zeta \to r/c_1$ and $\xi \to \cos \theta$. Also, as $\zeta \to \infty$ the potential with the spheroid present must approach the applied potential, so

$$\varphi_s = H_o c_1 [(1+\zeta^2)(1-\xi^2)]^{1/2} \cos \bar{\varphi} . \tag{29}$$

Thus it may be concluded from the form of the harmonic functions that m = 1 and n = 1. The expressions for the associated Legendre functions are

$$P_1'(\xi) = (1-\xi^2)^{1/2}$$

$$Q_1'(\xi) = (1-\xi^2)^{1/2} \left(\tfrac{1}{2} \ln \frac{1+\xi}{1-\xi} + \frac{\xi}{1-\xi^2} \right)$$

$$P_1'(j\zeta) = j(1+\zeta^2)^{1/2}$$

$$Q_1'(j\zeta) = (1+\zeta^2)^{1/2} \left(\cot^{-1}\zeta - \frac{\zeta}{1+\zeta^2} \right) .$$

Since the potential is finite when $\xi = \pm 1$, $Q_1'(\xi)$ must be excluded.

In Region I the potential is of the form

$$\varphi_s^I = P_1'(\xi)[AP_1'(j\zeta)+BQ_1'(j\zeta)] \cos \bar{\varphi}$$

$$= (1-\xi^2)^{1/2}[Aj(1+\zeta^2)^{1/2}+B(1+\zeta^2)^{1/2}(\cot^{-1}\zeta - \frac{\zeta}{1+\zeta^2})] \cos \bar{\varphi} \ . \qquad (30)$$

By letting $\zeta \to \infty$ it may be shown that

$$Aj = H_o c_1 \ .$$

Therefore the potential in the three regions must be of the form

$$\varphi_s^I = (1-\xi^2)^{1/2}(1+\zeta^2)^{1/2}[H_o c_1 + B(\cot^{-1}\zeta - \frac{\zeta}{1+\zeta^2})] \cos \bar{\varphi}$$

$$\varphi_s^{II} = (1-\xi^2)^{1/2}(1+\zeta^2)^{1/2}[Cj + D(\cot^{-1}\zeta - \frac{\zeta^2}{1+\zeta^2})] \cos \bar{\varphi}$$

$$\varphi_s^{III} = (1-\xi^2)^{1/2}(1+\zeta^2)^{1/2} Ej \cos \bar{\varphi} \ .$$

The function $Q_1'(j\zeta)$ must be excluded from Region III in order for H to be finite on the circle defined by $\xi = 0$, $\zeta = 0$. Applying the boundary conditions at the surfaces ζ_1 and ζ_2 the coefficients are determined to be

$$Ej = \frac{-2\mu D}{(1-\mu)\zeta_2(1+\zeta_2^2)}$$

$$Cj = -D\left[\cot^{-1}\zeta_2 + \frac{2\mu-(1-\mu)\zeta_2^2}{(1-\mu)\zeta_2(1+\zeta_2^2)}\right]$$

$$B = D\,\frac{1+\zeta_1^2}{2}\left[(1-\mu)\zeta_1(\cot^{-1}\zeta_1 - \cot^{-1}\zeta_2) + \frac{2\mu-(1-\mu)\zeta_1^2}{1+\zeta_1^2} - \frac{\zeta_1}{\zeta_2}\,\frac{2\mu-(1-\mu)\zeta_2^2}{1+\zeta_2^2}\right]$$

and

$$D = H_o c_1 / \left[(\cot^{-1}\zeta_1 - \cot^{-1}\zeta_2)\{1+(1-\mu)\frac{\zeta_1^2}{2} - (1-\mu)\zeta_1\frac{1+\zeta_1^2}{2}\cot^{-1}\zeta_1\}\right.$$

$$-(1-\mu)\frac{\zeta_1}{2}\left(1+\frac{1}{1+\zeta_1^2}\right) - \cot^{-1}\zeta_1\left\{\mu-(1-\mu)\frac{\zeta_1^2}{2}\right\}$$

$$\left.+\frac{2\mu-(1-\mu)\zeta_2^2}{1+\zeta_2^2}\left\{-\frac{1}{(1-\mu)\zeta_2} - \frac{\zeta_1^2}{2\zeta_2} + \frac{\zeta_1}{\zeta_2}\,\frac{1+\zeta_1^2}{2}\cot^{-1}\zeta_1\right\}\right] \ .$$

The flux density normal to the plane of the elliptical loop is

$$B_\varphi = \mu H_\varphi$$

evaluated at $\varphi = \pm \pi/2$. The total flux passing through the loop is

$$\Phi_s = -4c_1 \int_0^{\zeta_2} \int_0^1 \frac{\xi^2+\zeta^2}{(1+\zeta^2)(1-\xi^2)} \left.\frac{\partial \varphi_s^{III}}{\partial \varphi}\right|_{\varphi=\frac{\pi}{2}} d\xi\, d\zeta$$

$$-4\mu c_1 \int_{\zeta_2}^{\zeta_1} \int_0^1 \frac{\xi^2+\zeta^2}{(1+\zeta^2)(1-\xi^2)} \left.\frac{\partial \varphi_s^{II}}{\partial \varphi}\right|_{\varphi=\frac{\pi}{2}} d\xi\, d\zeta .$$

After substituting and integrating there results

$$\Phi_s = \pi\mu c_1 D\left[\zeta_1(1+\zeta_1^2)^{1/2}(\cot^{-1}\zeta_1 - \cot^{-1}\zeta_2) - (1+\zeta_1^2)^{1/2}\frac{\zeta_1}{\zeta_2}\frac{2\mu-(1-\mu)\zeta_2^2}{(1-\mu)(1+\zeta_2^2)} - \frac{2+\zeta_1^2}{(1+\zeta_1^2)^{1/2}}\right].$$

With the shell removed the total flux is

$$\Phi_0 = \pi abH_0 = \pi H_0 c_1^2 \zeta_1 (1+\zeta_1^2)^{1/2} .$$

The effective permeability for the oblate spheroidal shell is then given by

$$\mu_e = \mu \frac{\left[\cot^{-1}\zeta_1 - \cot^{-1}\zeta_2 + \frac{2\mu+(\mu-1)\zeta_2^2}{(\mu-1)\zeta_2(1+\zeta_2^2)} - \frac{2+\zeta_1^2}{\zeta_1(1+\zeta_1^2)}\right]}{\left[\begin{array}{l}(\cot^{-1}\zeta_1 - \cot^{-1}\zeta_2)\{1-(\mu-1)\frac{\zeta_1^2}{2}+(\mu-1)\zeta_1\frac{1+\zeta_1^2}{2}\cot^{-1}\zeta_1\} \\ +(\mu-1)\frac{\zeta_1}{2}\frac{2+\zeta_1^2}{1+\zeta_1^2} - \cot^{-1}\zeta_1\left\{\mu+(\mu-1)\frac{\zeta_1^2}{2}\right\} \\ +\frac{2\mu+(\mu-1)\zeta_2^2}{1+\zeta_2^2}\left\{\frac{1}{(\mu-1)\zeta_2} - \frac{\zeta_1^2}{2\zeta_2}+\frac{\zeta_1}{\zeta_2}\frac{1+\zeta_1^2}{2}\cot^{-1}\zeta_1\right\}\end{array}\right]} \qquad (31)$$

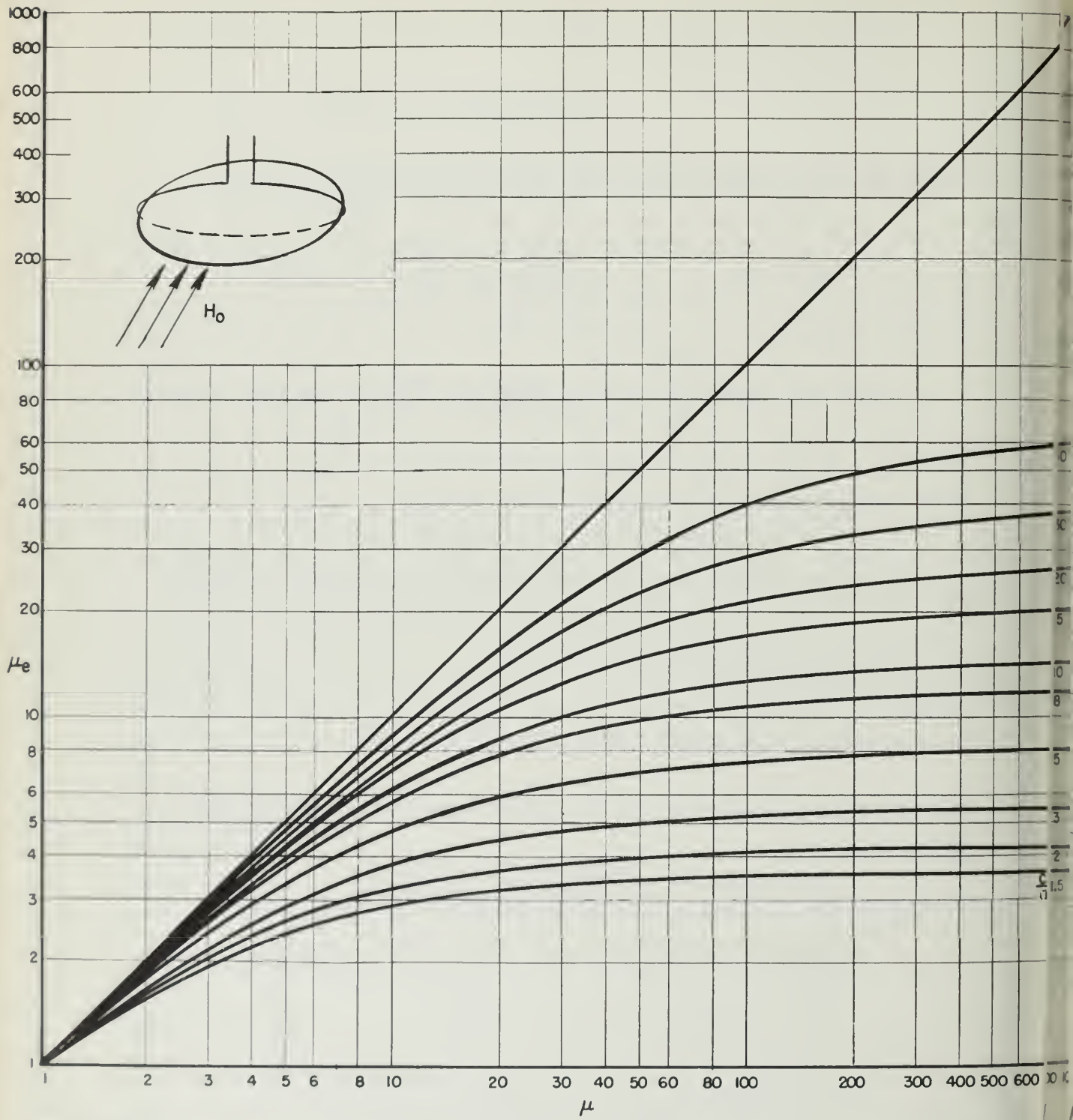

Figure 7a μ_e versus μ for a Solid Oblate Spheroid ($\acute{a}/a = 0$) for Various Diameter-to-Thickness Ratios

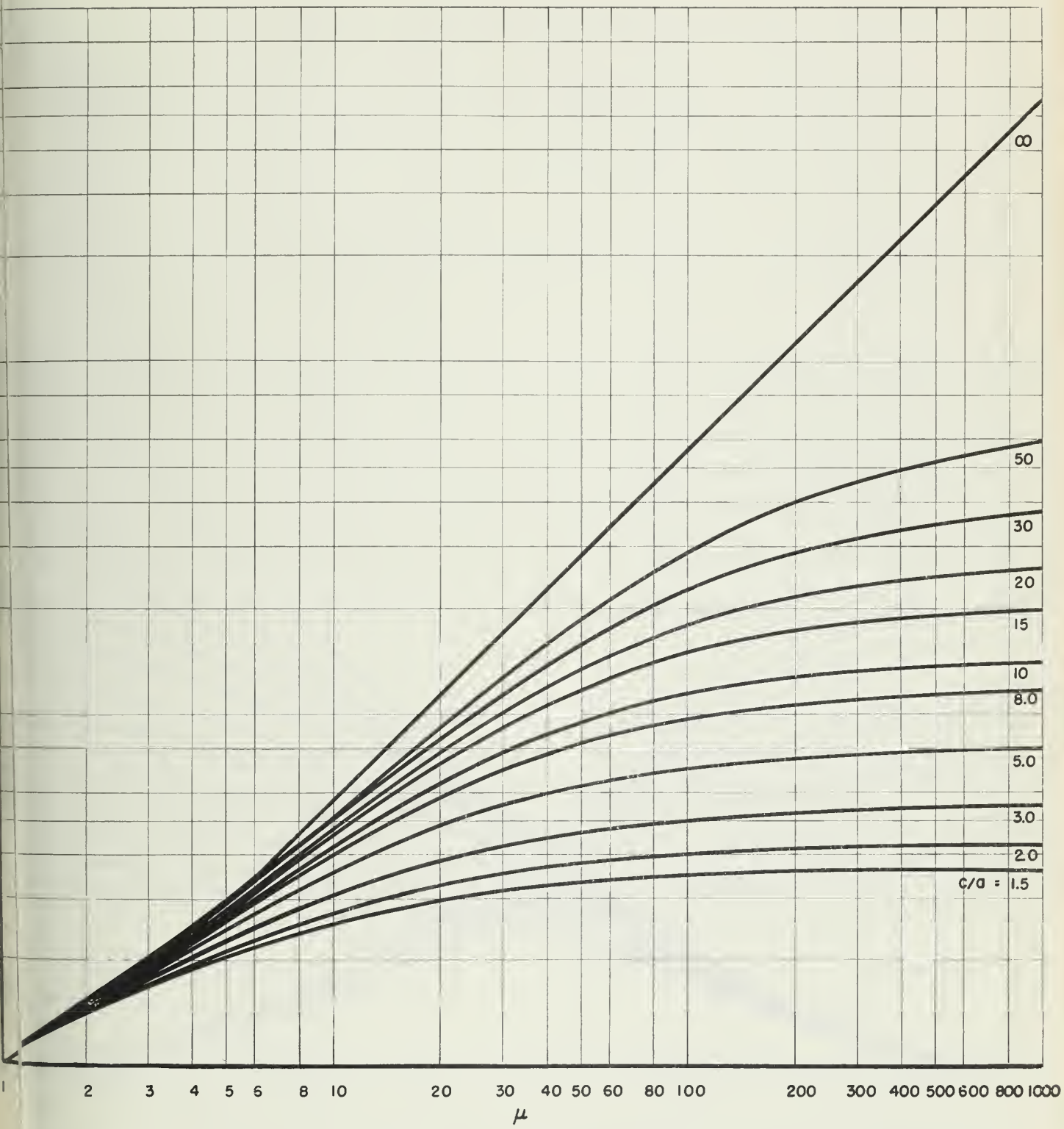

igure 7b μ_e versus μ for an Oblate Spheroidal Shell ($a'/a = 5$) for Various Diameter-to-Thickness Ratios

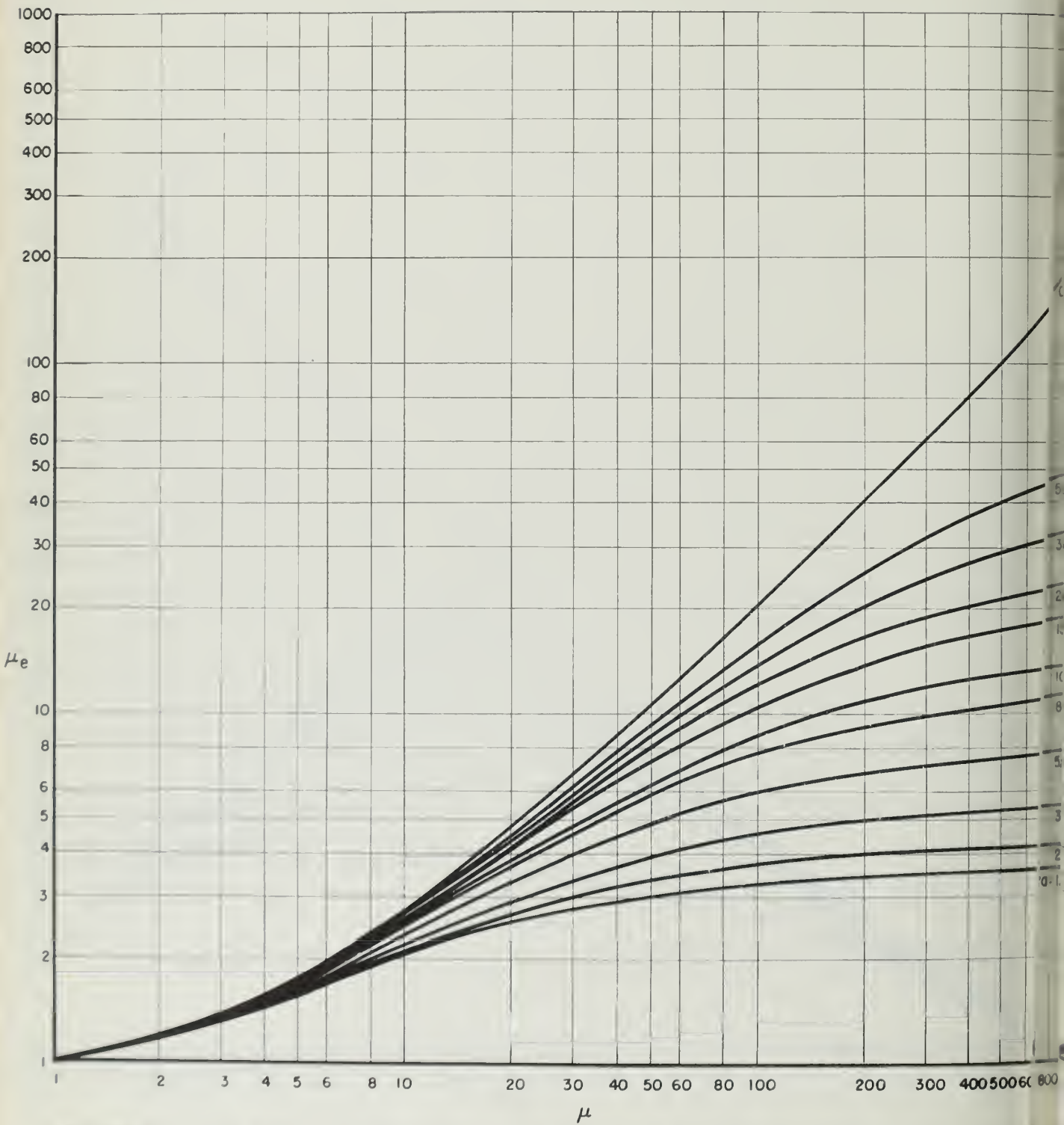

Figure 7c. μ_e versus μ for an Oblate Spheroidal Shell (a'/a = 8) for Various Diameter-Thickness Ratios

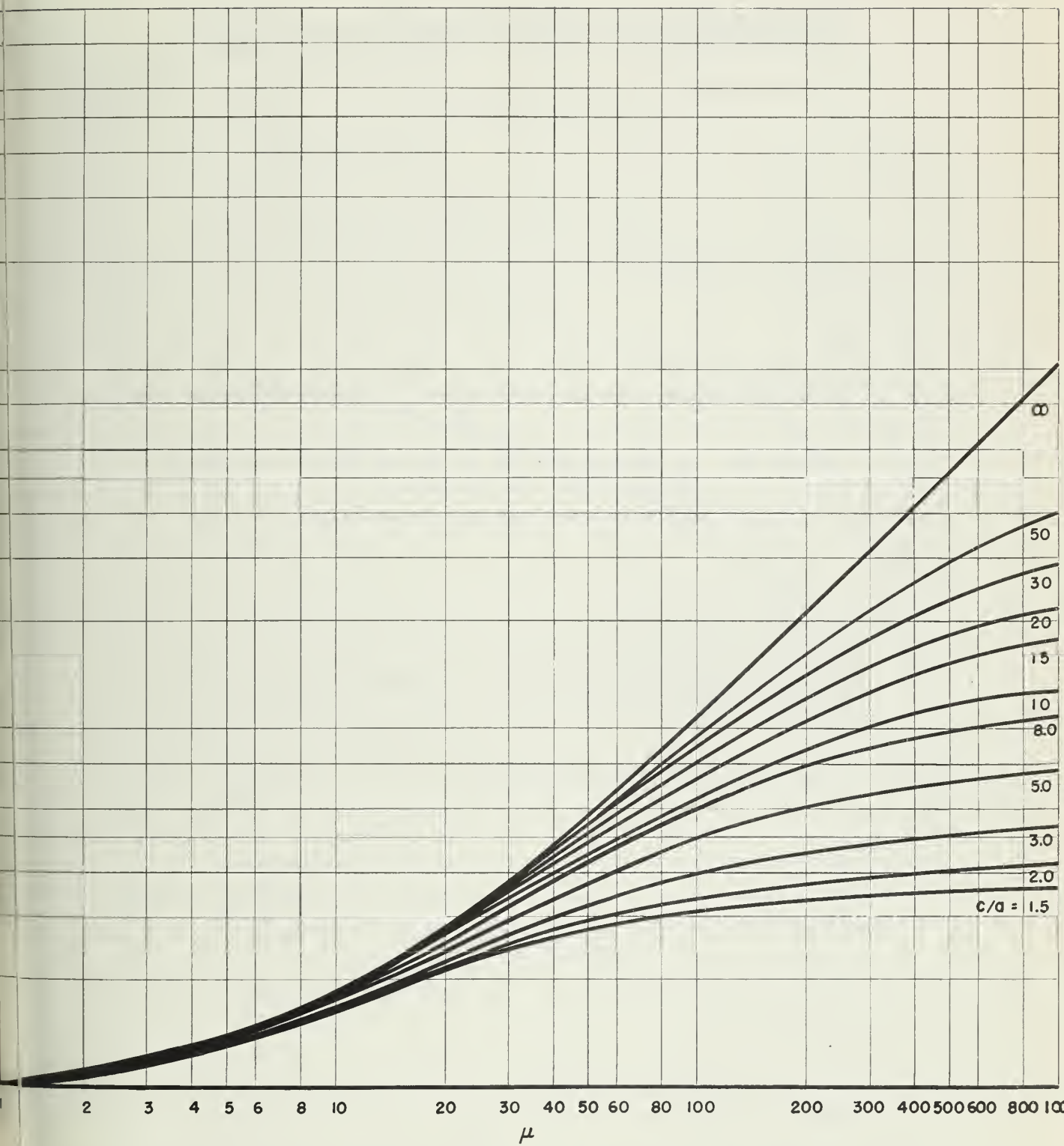

Figure 7d μ_e versus μ for an Oblate Spheroidal Shell ($\acute{a}/a$ = 9) for Various Diameter-to-Thickness Ratios

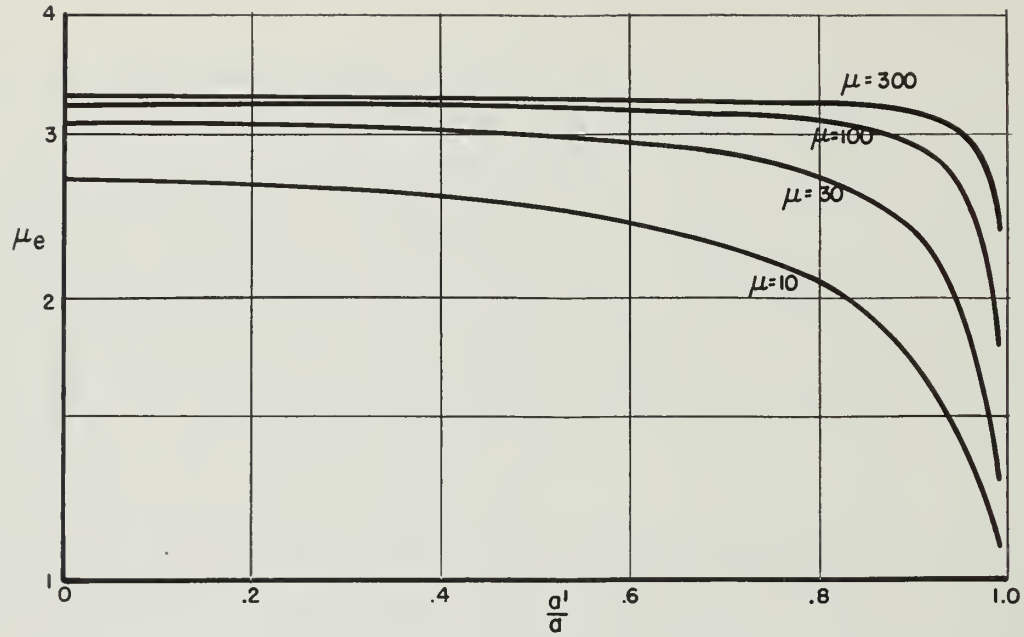

Figure 8a. μ_e versus a'/a for an Oblate Spheroidal Shell ($c/a = 1.25$) for Various μ

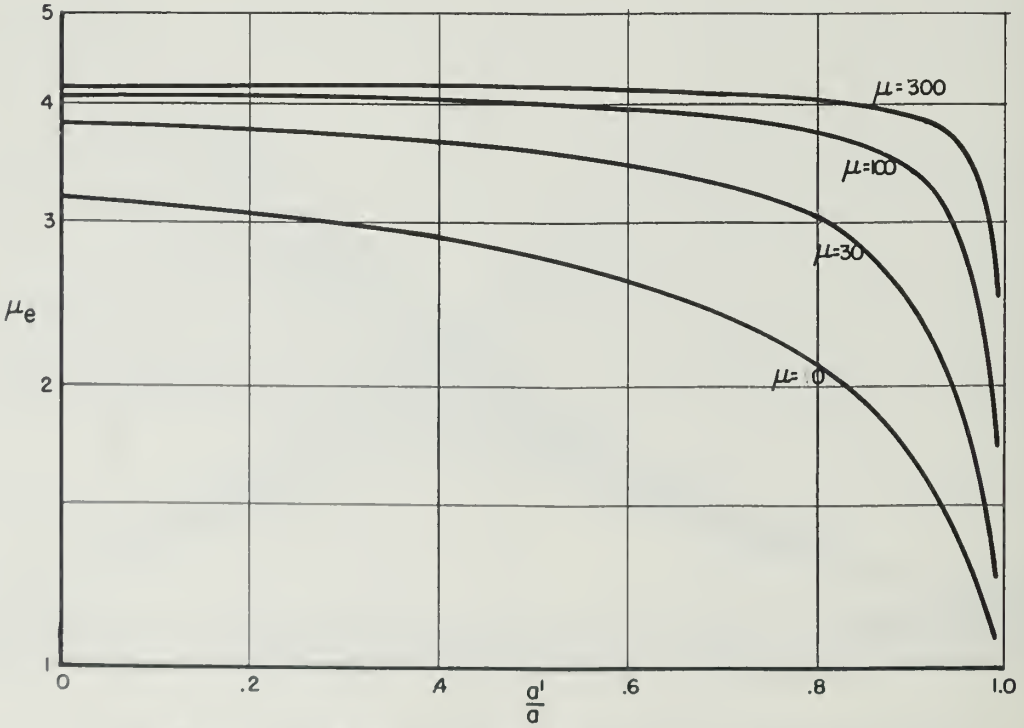

Figure 8b. μ_e versus a'/a for an Oblate Spheroidal Shell ($c/a = 2$) for Various μ

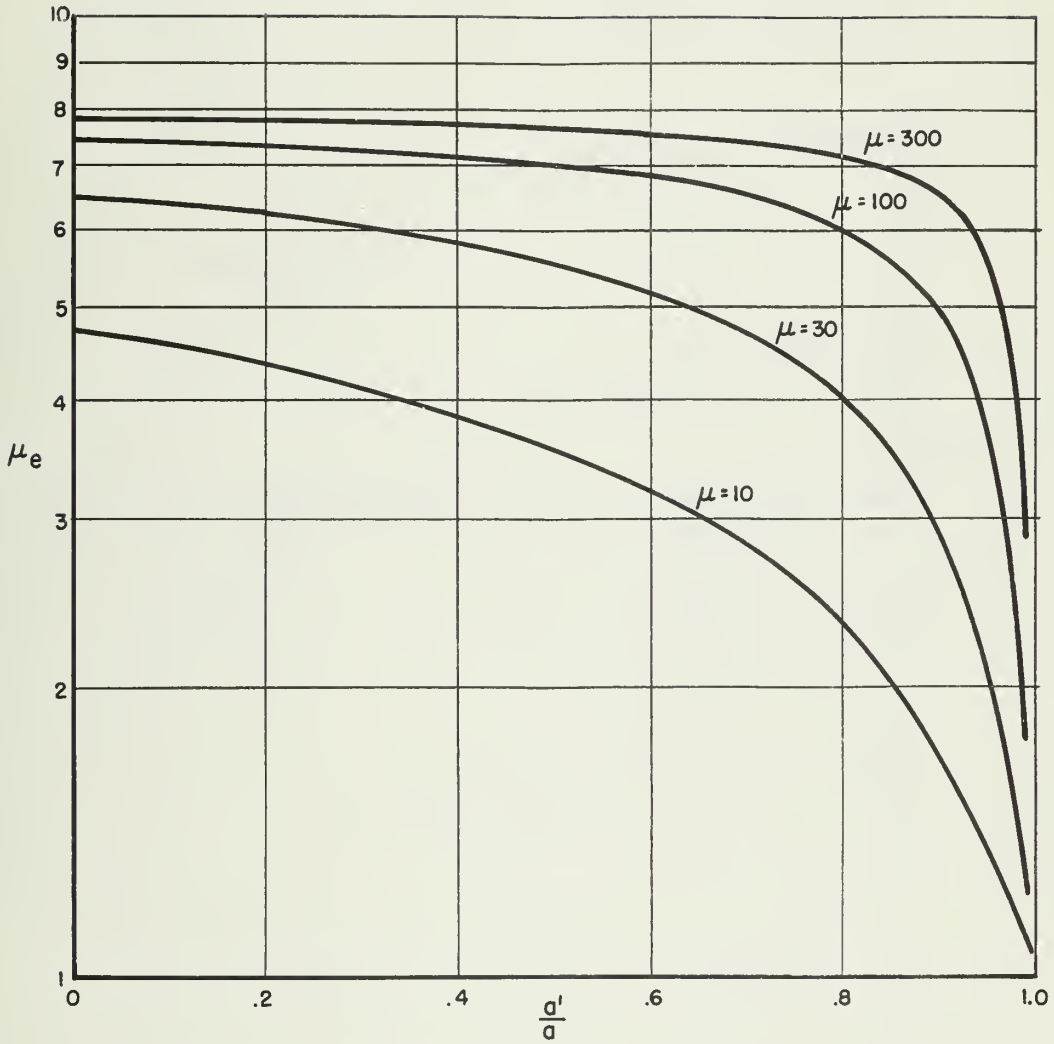

Figure 8c μ_e versus a'/a for an Oblate Sphercidal Shell ($c/a = 5$) for Various μ

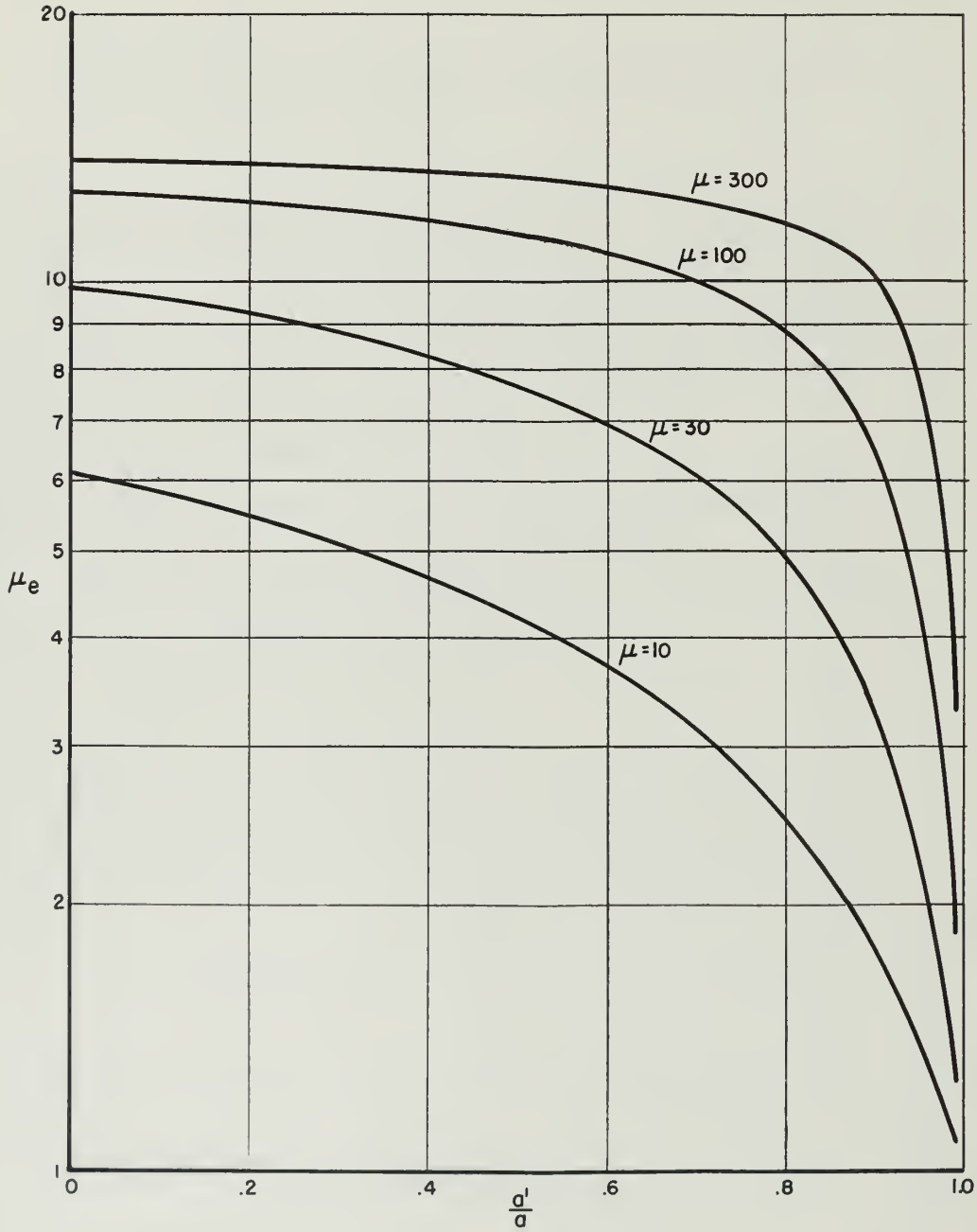

Figure 8d. μ_e versus a'/a for an Oblate Spheroidal Shell ($c/a = 10$) for Various μ

The limiting cases are given below. For the solid core

$$\lim_{a'/a \to 0} \mu_e = \frac{\mu}{1+(\mu-1)\frac{a}{2c_1}\left[\frac{c_2^2}{c_1^2}\cot^{-1}\frac{a}{c_1}-\frac{a}{c_1}\right]}$$

As $\mu \to \infty$ there results

$$\lim_{\mu \to \infty} \mu_e = \frac{1}{(ac^2/2c_1^3)\cot^{-1}(a/c_1)-(a^2/2c_1^2)} .$$

Also, as $c/a \to \infty$, we find that

$$\lim_{c/a \to \infty} \mu_e = (1-k)\mu+k .$$

Curves showing the variation of μ_e with μ for the oblate spheroidal shell are given in Figs. 7a to 7d. The variation of μ_e with the shell thickness is illustrated in Figs. 8a to 8d.

Next, consider the case of Fig. 9 when the applied uniform

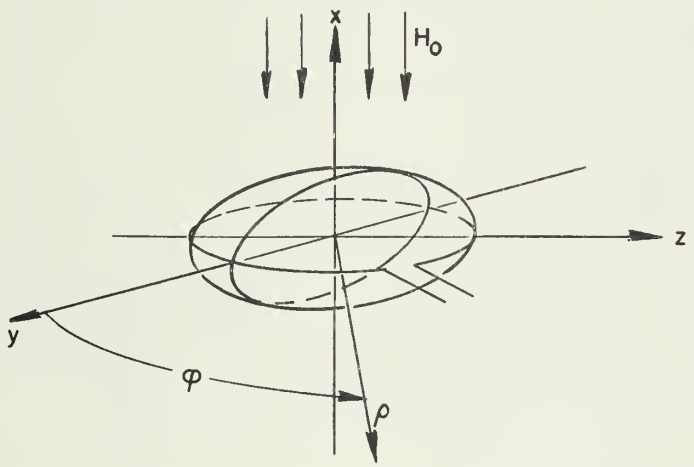

Figure 9. Uniform Magnetic Field Applied to an Oblate Spheroidal Shell with a Circular Loop Placed in the yz Plane

magnetic field is in the negative x direction and a circular loop lying in the yz plane is placed around the spheroid. Since there is no variation with φ for this case, the potential will take the following general form:

$$\varphi = P_1(\xi)[AP_1(j\zeta)+BQ_1(j\zeta)].$$

Following the same procedure as before, there results

$$\mu_e = \mu \frac{\left[\cot^{-1}\zeta_1-\cot^{-1}\zeta_2+\frac{\zeta_2}{1+\zeta_2^2}-\frac{\zeta_1}{1+\zeta_1^2}-\frac{1}{(\mu-1)\zeta_2(1+\zeta_2^2)}\right]}{\left[\frac{(\mu-1)\zeta_2^2-1}{(\mu-1)\zeta_2(\zeta_2^2+1)}-\cot^{-1}\zeta_2 + (\zeta_1\cot^{-1}\zeta_1-1)\left\{(\mu-1)\zeta_1-(\mu-1)(\zeta_1^2+1)(\cot^{-1}\zeta_1-\cot^{-1}\zeta_2) - \frac{(\zeta_1^2+1)[(\mu-1)\zeta_2^2-1]}{\zeta_2(\zeta_2^2+1)}\right\}\right]} .$$

For the solid core, there results

$$\lim_{a'/a \to 0} \mu_e = \frac{\mu}{1+(\mu-1)\frac{c^2}{c_1^2}\left(1-\frac{a}{c_1}\cot^{-1}\frac{a}{c_1}\right)} .$$

Also, for the shell,

$$\lim_{\mu \to \infty} \mu_e = \frac{c_1^2}{c^2}\frac{1}{1-\frac{a}{c_1}\cot^{-1}\frac{a}{c_1}} .$$

Figure 10 shows the variation of μ_e versus μ for different values of the ratio a/c in the case of a solid oblate spheroid. The variation of μ_e versus shell thickness for a fixed ratio, c/a = 2, and different values of μ is illustrated in Fig. 11.

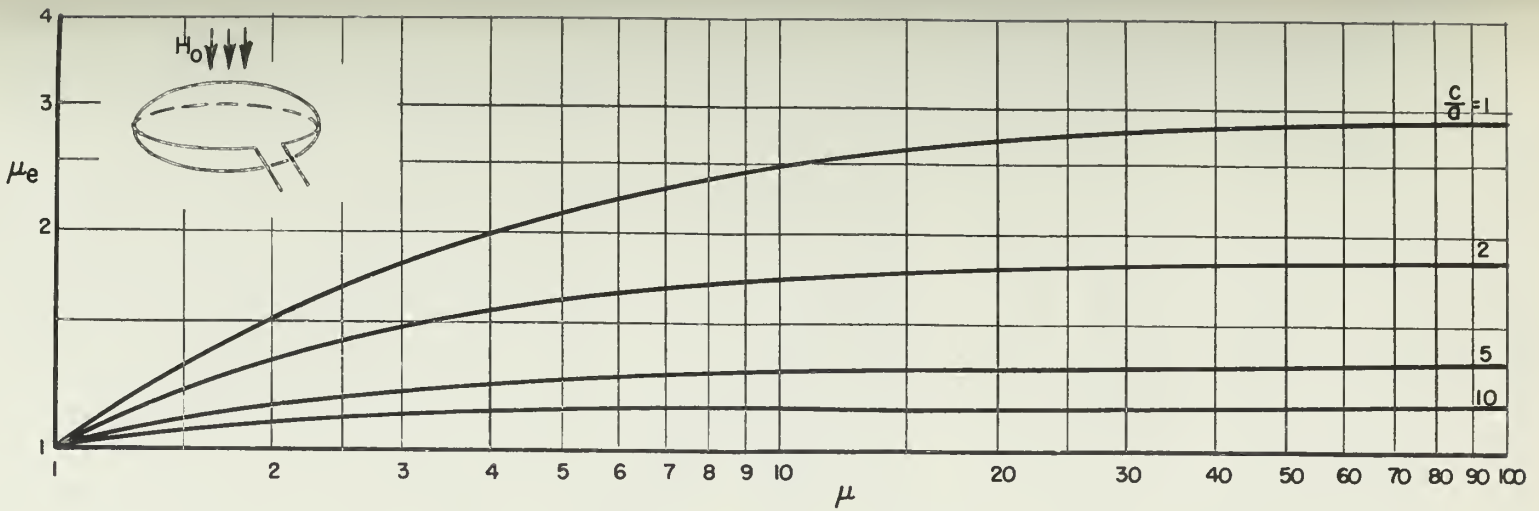

Figure 10. μ_e versus μ for a Solid Oblate Spheroid for Various Diameter-to-Thickness Ratios (c/a)

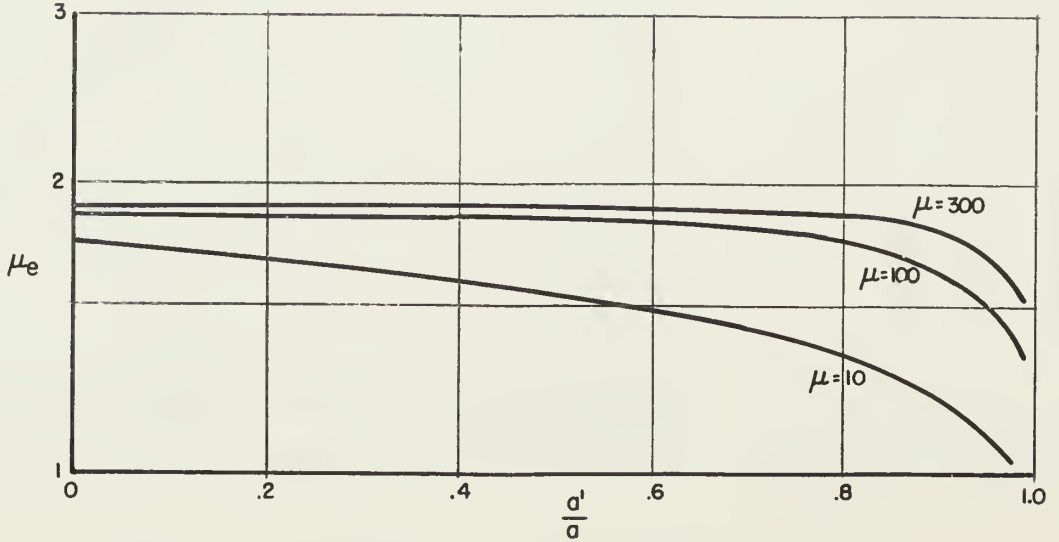

Figure 11 μ_e versus a'/a for an Oblate Spheroidal Shell ($c/a = 2$) for Various μ

4. APPLICATION TO LOOP ANTENNA DESIGN

The design of the winding for a ferrite loop antenna is just as important as the design of the core. However, since there are various factors to consider in the design of the winding, such as the type and size of the conductor and the number and distribution of the turns, a simple loop wound around the central cross section of the core has been assumed in order to compare the different cores.

The prolate spheroid is not an accurate approximation to the cylindrical rod. A slightly larger length-to-diameter ratio is required for a prolate spheroid than for a rod of identical material in order to have the same effective permeability. The curves of Fig. 12

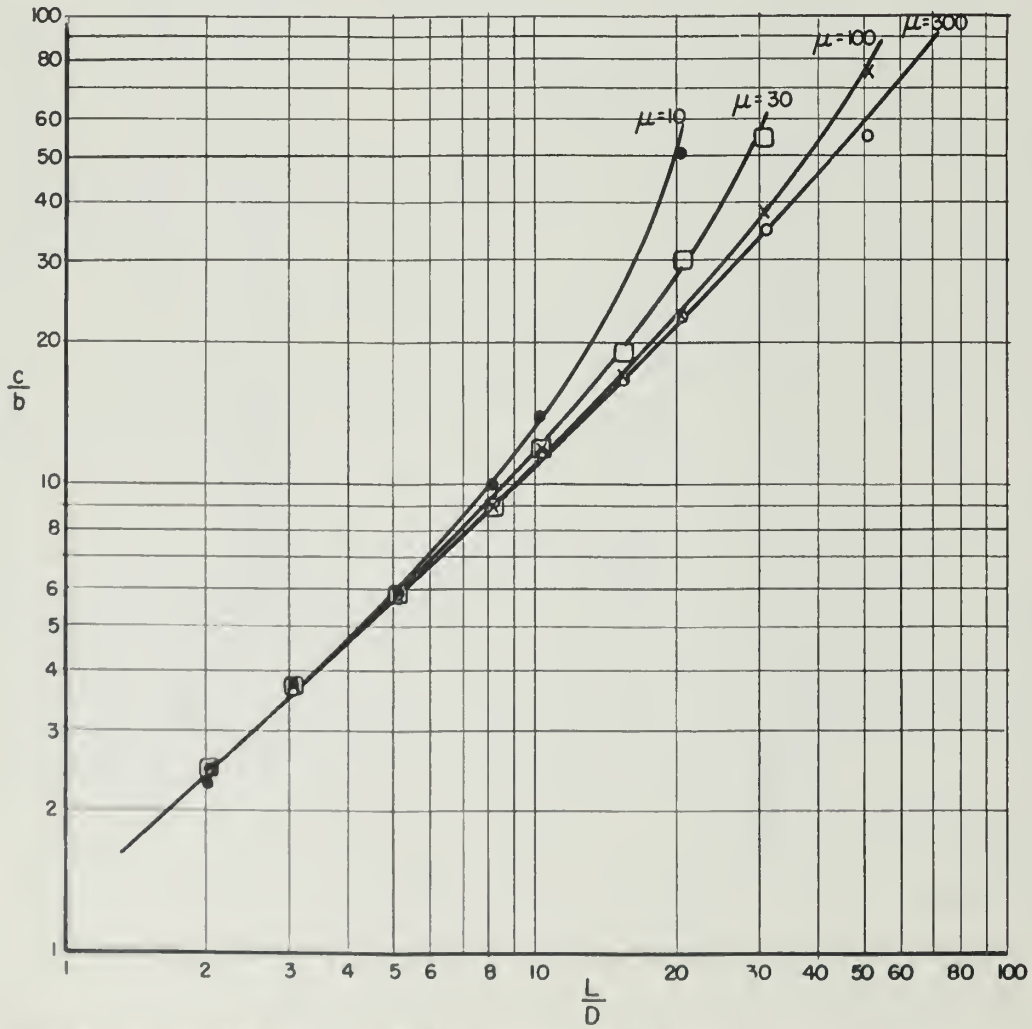

Figure 12 Curves Showing the Length-to-Diameter Ratio c/b, of a Solid Prolate Spheroid Required to Produce the Same Effective Permeability as a Solid Cylindrical Rod with a Length-to-Diameter Ratio of L/D

illustrate this for the solid prolate spheroid and for the cylindrical rod. Although the curves are not exact for shell type cores, they may be used to improve the accuracy of estimating μ_e for a tubular cylindrical core. That is, given a tube with a certain length-to-diameter ratio, L/D, the corresponding length-to-diameter ratio, c/b, of the spheroid would be read from Fig. 12. Then, using the same shell thickness, μ_e would be determined from Figs. 3 or 4.

The most important factor to consider in a loop design is the efficiency or the signal-to-noise ratio which is proportional to the efficiency. The efficiency is defined by

$$\text{Eff} = \frac{R_r}{R_{in}}$$

where R_r is the radiation resistance and R_{in} is the input resistance of the loop. For the comparison of the cores, the important parameters to consider are the μ_e of the core and the area, A, of the loop, since the radiation resistance is proportional to

$$R_r \propto (A\mu_e)^2 .$$

The input resistance is due to losses in the loop conductor and the core, as well as to the radiation. For electrically small loops the radiation resistance is negligible compared to the conductor and equivalent core resistance. (Loop efficiencies of 10^{-6} are common.) The conductor losses are proportional to the length of the loop wire and also depend to a lesser extent, but in a complex manner, upon the geometry and construction of the winding and the core. The core losses also depend upon the type of winding and the shape of the core. Thus it would be very difficult to use loop efficiency as a basis of comparison of various cores. For simplicity, then, the square of the factor $A\mu_e$ will be used as a basis of comparison. If the core loss is negligible compared to the conductor loss (as it sometimes is for ferrite loops at frequencies below 10 mc) then this is a good basis for comparison because the conductor loss is, to the first order, independent of the loop size and core shape, for a given loop inductance, i.e., the loop efficiency is approximately proportional to

$(A\mu_e)^2$. On the other hand, if the conductor loss is negligible compared to the core loss (as it may be for frequencies above 10 mc or for some ferrite materials) this is a poor basis for comparison because the core loss is approximately proportional to[4]

$$R_{core} \propto \mu_e{}^2 A(1-1/\mu_e)$$

Thus the efficiency would be nearly independent of the core shape, especially for large μ_e. Unfortunately, the core and conductor losses are of the same order of magnitude for many cases so that it is even more difficult to make theoretical comparisons.

Consider first the case when the volume of a solid core is held constant but the length-to-diameter or diameter-to-thickness ratio is allowed to vary. Curves of $(A\mu_e)^2$ versus the ratio c/b for a prolate spheroid and c/a for an oblate spheroid are shown in Fig. 13. The scales of c/b and c/a are arranged so that the loop area for prolate and oblate spheroids is the same for any one abscissa. However, since the loop is assumed to be tightly wound around the spheroid and since the volume of the core is held constant, the loop area decreases with increasing abscissa. Two important conclusions may be drawn from these curves. First, for a given volume of core material there are optimum values of the ratios c/b and c/a for the prolate and oblate spheroids, respectively. The optimum value depends upon the permeability of the material. For materials with a high permeability it may not be practical to use the optimum ratio (for example, with μ = 100, a c/a ratio of 150 would be required). Second, for a given volume of core material the oblate shape is preferable since the value of $(A\mu_e)^2$ is up to three times greater than that for the prolate shape.

Next, consider the case for which the major axis of a solid core is held constant and the other parameters (the volume and minor axis) are allowed to vary. This condition would apply to a flush-mounted ferrite loop placed in a cylindrical cavity of fixed diameter. Figure 14 shows $(A\mu_e)^2$ as a function of c/b and c/a for the prolate and oblate spheroids, respectively. For these curves the length of the prolate spheroid and the diameter of the oblate spheroid are held

4 This result is to be published shortly in an Antenna Laboratory Report by W. L. Weeks on ferrite loop antennas.

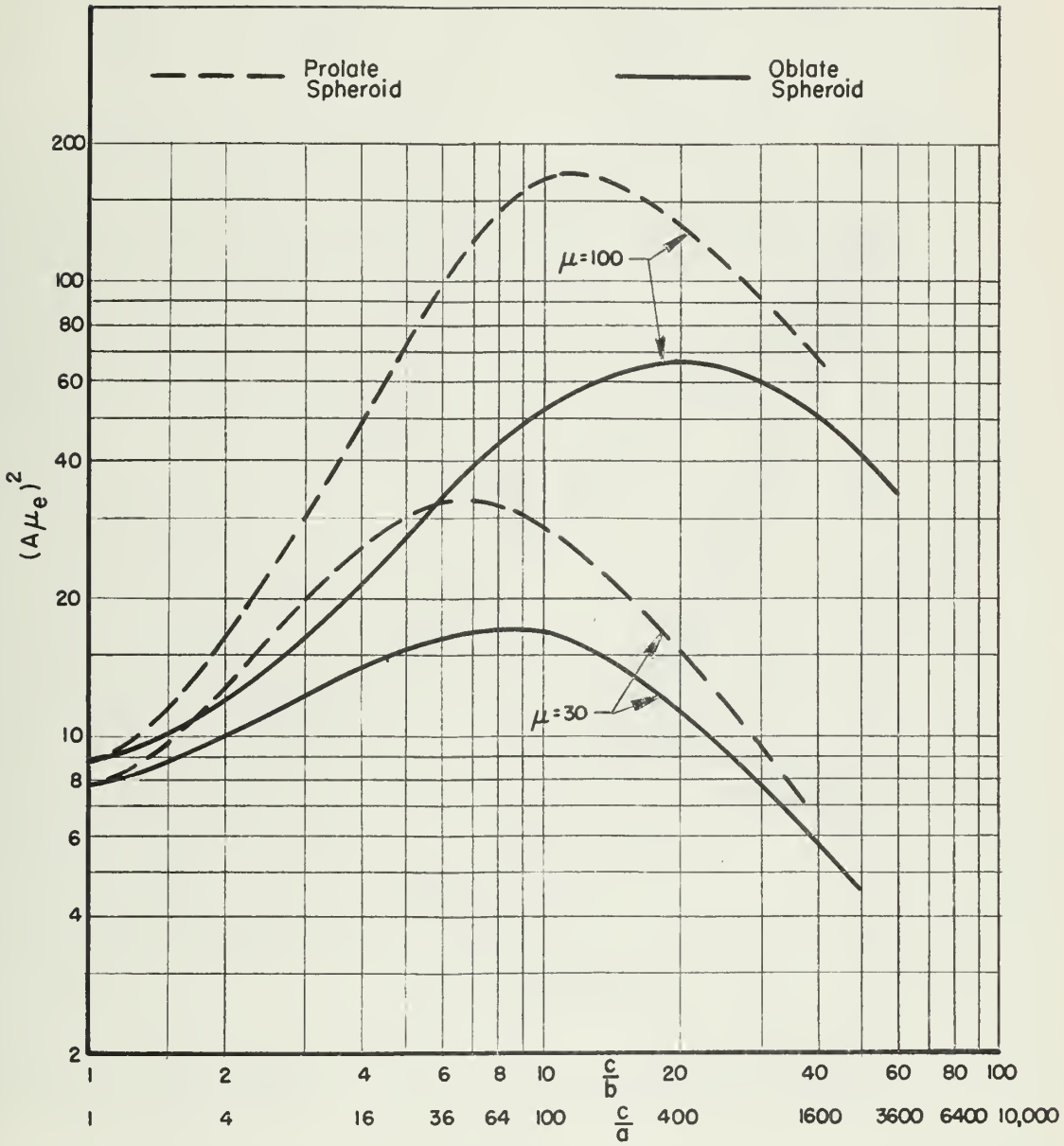

Figure 13 Plot of $(A\mu_e)^2$ versus c/b for the Prolate Spheroid and c/a for the Oblate Spheroid (The volume of the core is held constant and the area of the loop for the prolate and oblate spheroid is identical for any one abscissa However the loop area for both varies with the abscissa)

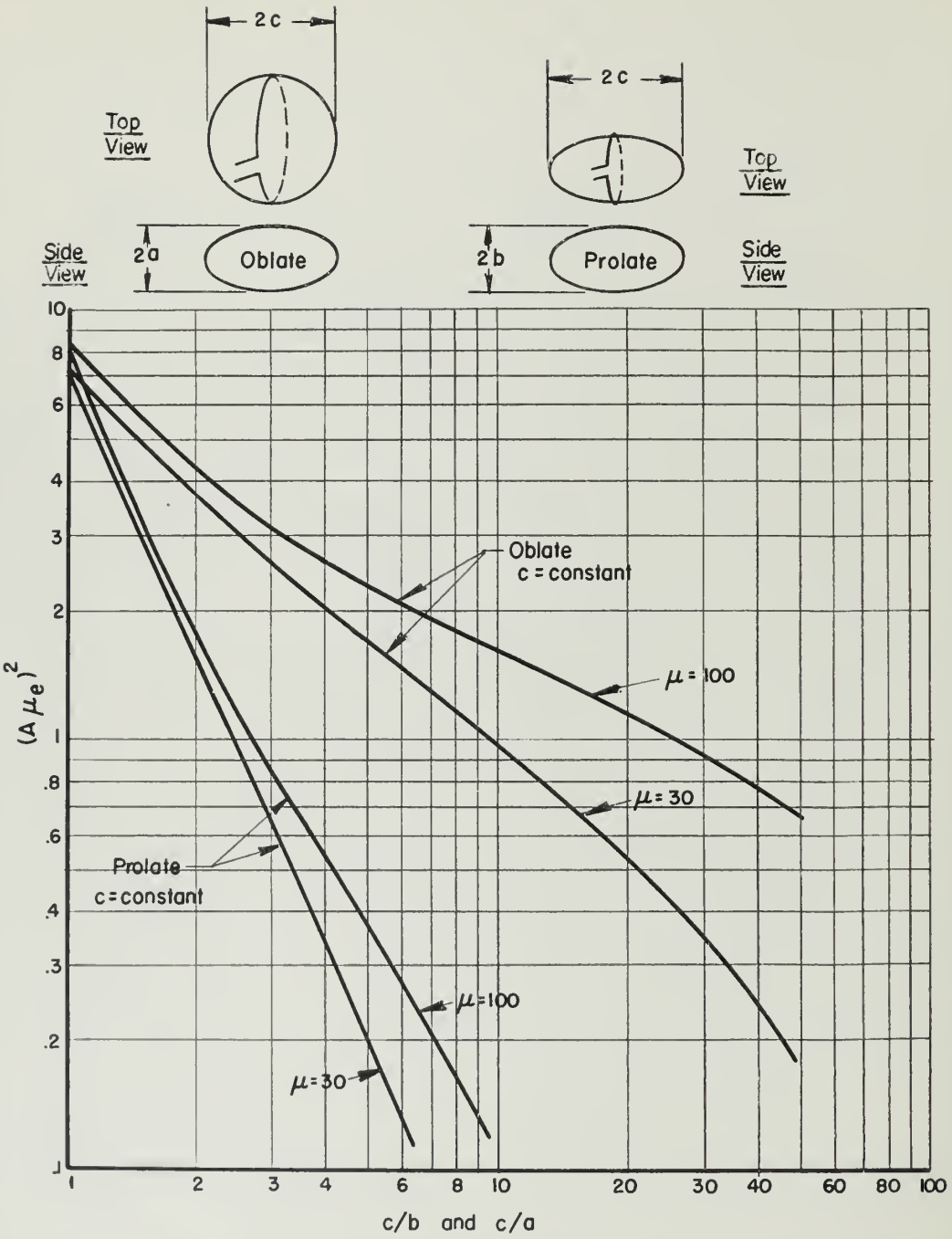

Figure 14 Plot of $(A\mu_e)^2$ versus c/b and c/a for the Solid Prolate and Oblate Spheroidal Cores with c Held Constant

constant. The volume of the core decreases with increasing abscissa. It is seen that the spherical shape has the largest value of $(A\mu_e)^2$. This is to be expected since the loop area and volume of the core are maximum for this case. Also, it is apparent that when c/b and c/a are equal, the oblate shape is better than the prolate shape. For example, for c/a = c/b = 10 the value of $(A\mu_e)^2$ for the oblate is 15 times that for the prolate spheroid for $\mu = 100$. This is due to the fact that the loop area and core volume for the oblate core are ten times greater than those for the prolate core.

Consider now a prolate core with constant length and volume of material, but let the shell thickness change. Figure 15 illustrates the variation of $(A\mu_e)^2$ and the shell thickness as a function of the length-to-diameter ratio. Again it will be noticed that as the spherical shape is approached, $(A\mu_e)^2$ increases rapidly.

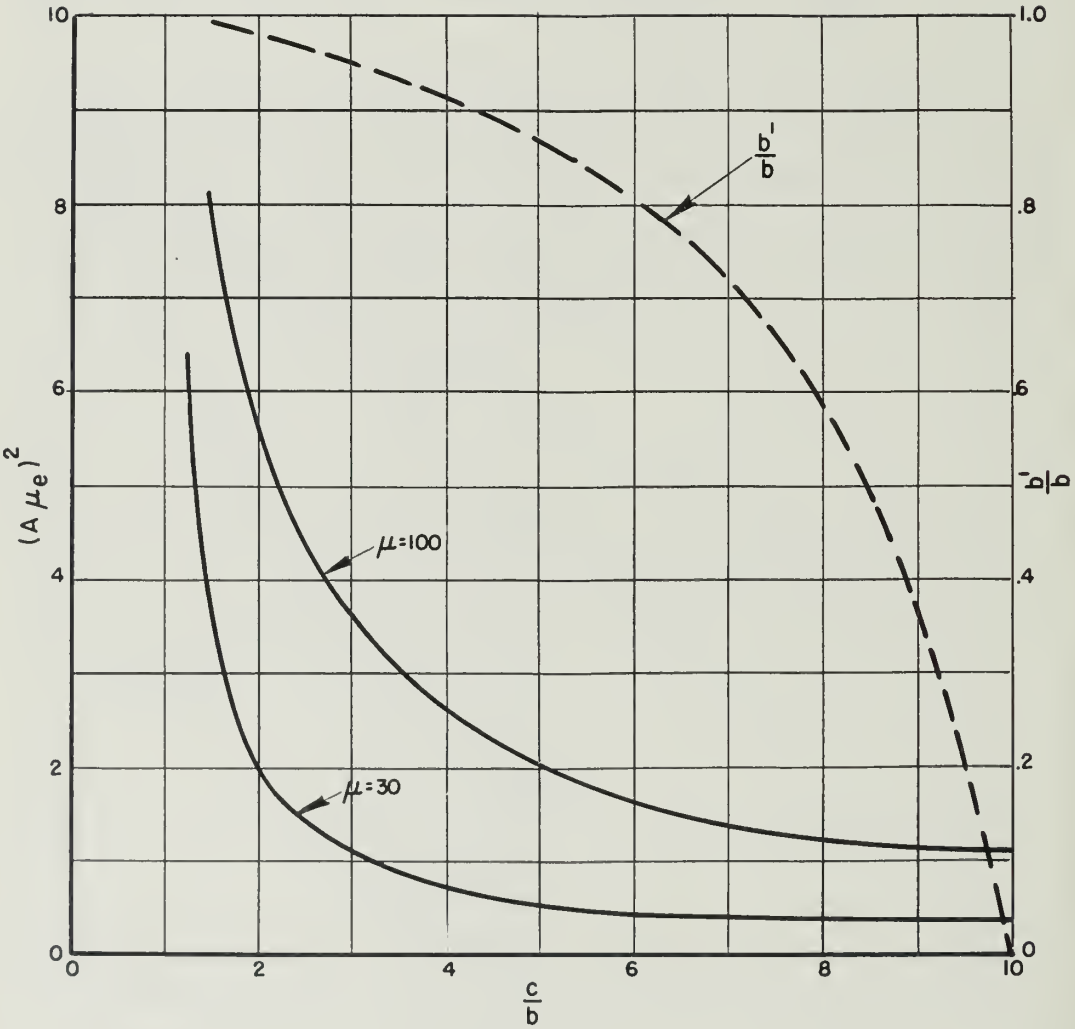

Figure 15 Plot of $(A\mu_e)^2$ versus c/b for a Prolate Spheroidal Core with c and the Core Volume Held Constant

5. CONCLUSIONS

The sets of curves illustrating the variation of μ_e versus the shell thickness and length-to-diameter ratio for prolate and oblate spheroidal shells are quite useful for comparing the effectiveness of various types of cores. For airborne ferrite loop applications where the length, height, and weight are limited, the following rules of thumb may be applied. First, make the loop area as large as possible. Next, use the maximum weight of core material allowed and distribute it in a shell form which just fits inside of the loop. For rotating or crossed loop applications this will usually result in an oblate spheroidal shell type of core with an elliptical loop.

6. ACKNOWLEDGMENT

It is a pleasure to acknowledge the work of Mr. Earl J. Schweppe who evaluated the expressions for the effective permeability by means of the Illiac digital computer.

DISTRIBUTION LIST FOR TECHNICAL REPORTS ISSUED UNDER CONTRACT AF33(616)-3220

One copy each unless otherwise indicated

Contractor
Wright Air Development Center
Wright-Patterson Air Force Base, Ohio

Attn: Mr. E. M. Turner, WCLRS-6
4 copies

Commander
Wright Air Development Center
Wright-Patterson Air Force Base, Ohio

Attn: Mr. N. Draganjac, WCLNT-4

Armed Services Technical Information Agency
Knott Building
4th and Main Streets 5 copies
Dayton 2, Ohio 1 repro.

Attn: DSC-SA (Reference AFR205-43)

Commander
Hq. A. F. Cambridge Research Center
Air Research and Development Command
Laurence G. Hanscom Field
Bedford, Massachusetts

Commander
Hq. A.F. Cambridge Research Center
Air Research and Development Command
Laurence G. Hanscom Field
Bedford, Massachusetts

Attn: CRTOTL-1

Commander
Hq. A.F. Cambridge Research Center
Air Research and Development Command
Laurence G. Hanscom Field
Bedford, Massachusetts

Attn: CRRD, R. E. Hiatt

Air Force Development Field
Representative
Attn: Major M. N. Abramovich
Code 1110
Naval Research Laboratory
Washington 25, D. C.

Director
Ballistics Research Lab.
Aberdeen Proving Ground, Maryland

Attn: Ballistics Measurement Lab.

Office of the Chief Signal Officer
Attn: SIGNET-5
Eng. & Technical Division
Washington 25, D. C.

Commander
Rome Air Development Center
Attn: RCERA-1 D. Mather
Griffiss Air Force Base
Rome, New York

Director
Evans Signal Laboratory
Belmar, New Jersey

Attn: Mr. O. C. Woodyard

Director
Evans Signal Laboratory
Belmar, New Jersey

Attn: Mr. S. Krevsky

Director
Evans Signal Laboratory
Belmar, New Jersey

Attn: Technical Document Center

Naval Air Missile Test Center
Point Mugu, California

Attn: Antenna Section

Commander
U. S. Naval Air Test Center
Attn: ET-315
Antenna Section
Patuxent River, Maryland

DISTRIBUTION LIST (Cont.)

Beech Aircraft Corporation
Attn: Chief Engineer
6600 E. Central Avenue
Wichita 1, Kansas
M/F Contract AF33(600)-20910

Bell Aircraft Corporation
Attn: Mr. J. D. Shantz
Buffalo 5, New York
M/F Contract W-33(038)-14169

Boeing Airplane Company
Attn: G. L. Hollingsworth
7755 Marginal Way
Seattle, Washington
M/F Contract AF33(038)-21096

Grumman Aircraft Engineering Corp.
Attn: J. S. Erickson,
Chief Engineer
Bethpage
Long Island, New York
M/F Contract NOa(s) 51-118

Hallicrafters Corporation
Attn: Norman Foot
440 W. 5th Avenue
Chicago, Illinois
M/F Contract AF33(600)-26117

Hoffman Laboratories, Inc.
Attn: Markus McCoy
Los Angeles, California
M/F Contract AF33(600)-17529

Hughes Aircraft Corporation
Division of Hughes Tool Company
Attn: Dr. Vanatta
Florence Avenue at Teale
Culver City, California
M/F Contract AF33(600)-27615

Johns Hopkins University
Radiation Laboratory
Attn: Dr. D. D. King
1315 St. Paul Street
Baltimore 2, Maryland
M/F Contract AF33(616)-68

Fairchild Engine & Airplane Corp.
Fairchild Airplane Division
Attn: L. Fahnestock
Hagerstown, Maryland
M/F Contract AF33(038)-18499

Federal Telecommunications Lab.
Attn: Mr. A. Kandoian
500 Washington Avenue
Nutley 10, New Jersey
M/F Contract AF33(038)-13289

Glenn L. Martin Company
Attn: N. M. Voorhies
Baltimore 3, Maryland
M/F Contract AF33(600)-21703

Massachusetts Institute of Tech.
Attn: Prof. H. J. Zimmermann
Research Lab. of Electronics
Cambridge, Massachusetts
M/F Contract AF33(616)-2107

North American Aviation, Inc.
Aerophysics Laboratory
Attn: Dr. J. A. Marsh
12214 Lakewood Boulevard
Downey, California
M/F Contract AF33(038)-18319

North American Aviation, Inc.
Los Angeles International Airport
Attn: Mr. Dave Mason
Engineering Data Section
Los Angeles 45, California
M/F Contract AF33(038)-18319

Northrop Aircraft Incorporated
Attn: Northrop Library
Dept. 2135
Hawthorne, California
M/F Contract AF33(600)-22313

Ohio State Univ. Research Foundation
Attn: Dr. T. C. Tice
310 Administration Bldg.
Ohio State University
Columbus 10, Ohio
M/F Contract AF18(600)-85

Commander
Air Force Missile Test Center
Patrick Air Force Base, Florida

Attn: Technical Library

Chief
BuShips, Room 3345
Department of the Navy
Attn: Mr. A. W Andrews
Code 883
Washington 25, D. C

Director
Naval Research Laboratory
Attn: Dr. J. I. Bohnert
Anocostia
Washington 25, D. C.

National Bureau of Standards
Department of Commerce
Attn: Dr. A. G. McNish
Washington 25, D. C.

Director
U.S. Navy Electronics Lab.
Attn: Dr. T. J. Keary
Code 230
Point Loma
San Diego 52, California

Chief of Naval Research
Department of the Navy
Attn: Mr. Harry Harrison
Code 427, Room 2604
Bldg. T-3
Washington 25, D. C

Airborne Instruments Lab., Inc.
Attn: Dr. E. G. Fubini
Antenna Section
160 Old Country Road
Mineola, New York
M/F Contract AF33(616)-2143

Andrew Alford Consulting Engrs.
Attn: Dr. A. Alford
299 Atlantic Ave.
Boston 10, Massachusetts
M/F Contract AF33(038)-23700

Chief
Bureau of Aeronautics
Department of the Navy
Attn: W. L. May, Aer-EL-4114
Washington 25, D. C.

Chance-Vought Aircraft Division
United Aircraft Corporation
Attn: Mr. F. N. Kickerman
Thru: BuAer Representative
Dallas, Texas

Consolidated-Vultee Aircraft Corp.
Attn: Dr. W. J. Schart
San Diego Division
San Diego 12, California
M/F Contract AF33(600)-26530

Consolidated-Vultee Aircraft Corp.
Fort Worth Division
Attn: C. R. Curnutt
Fort Worth, Texas
M/F Contract AF33(038)-21117

Textron American, Inc. Div.
Dalmo Victor Company
Attn: Mr. Glen Walters
1414 El Camino Real
San Carlos, California
M/F Contract AF33(038)-30525

Dorne & Margolin
30 Sylvester Street
Westbury
Long Island, New York
M/F Contract AF33(616)-2037

Douglas Aircraft Company, Inc.
Long Beach Plant
Attn: J. C. Buckwalter
Long Beach 1, California
M/F Contract AF33(600)-25669

Electronics Research, Inc.
2300 N. New York Avenue
P. O. Box 327
Evansville 4, Indiana
M/F Contract AF33(616)-2113

DISTRIBUTION LIST (Cont.)

Land-Air Incorporated
Cheyenne Division
Attn: Mr. B.L. Michaelson
Chief Engineer
Cheyenne, Wyoming
M/F Contract AF33(600)-22964

Lockheed Aircraft Corporation
Attn: C. L. Johnson
P. O. Box 55
Burbank, California
M/F NOa(S)-52-763

McDonnell Aircraft Corporation
Attn: Engineering Library
Lambert Municipal Airport
St. Louis 21, Missouri
M/F Contract AF33(600)-8743

Michigan, University of
Aeronautical Research Center
Attn: Dr. R.D. O'Neill
Willow Run Airport
Ypsilanti, Michigan
M/F Contract AF33(038)-21573

Chief
Bureau of Ordnance
Department of the Navy
Attn: A.D. Bartelt
Washington 25, D. C.

Radioplane Company
Van Nuys, California
M/F Contract AF33(600)-23893

Raytheon Manufacturing Company
Attn: Dr. H.L. Thomas
Documents Section
Waltham 54, Massachusetts
M/F Contract AF33(038)-13677

Republic Aviation Corporation
Attn: Engineering Library
Farmingdale
Long Island, New York
M/F Contract AF33(038)-14810

Ryan Aeronautical Company
Lindbergh Drive
San Diego 12, California
M/F Contract W-33(038)-ac-21370

Sperry Gyroscope Company
Attn: Mr. B. Berkowitz
Great Neck
Long Island, New York
M/F Contract AF33(038)-14524

Temco Aircraft Corp
Attn: Antenna Design Group
Dallas, Texas
M/F Contract AF33(600)-31714